Monograph:
Edwards, J.B. (1979) Modelling of Coal and Mineral Extraction Processes. Research Report. ACSE Research Report 105 . Department of Automatic Control and Systems Engineering

MODELLING OF COAL AND MINERAL EXTRACTION PROCESSES

by

J.B. Edwards, B.Sc.(Eng.), M.Sc., C.Eng., M.I.E.E., A.M.E.M.E.

Senior Lecturer in the Department of Control Engineering,
University of Sheffield,
Mappin Street,
Sheffield S1 3JD.

Research Report No. 105

September 1979

To be published in the textbook "Modelling of Dynamical Systems"
(Editor: Professor H. Nicholson), Peter Peregrinus, 1980.

Modelling of Coal and Mineral Extraction Processes

13.1 Introduction

Mining involves the following fundamental operations:

(a) the actual winning of the coal, stone or mineral ore from the underground seam of vein in which it naturally occurs,

(b) the clearance of the material from several such sources in any one mine to some central point for the final operation:

(c) the preparation of the extracted raw material for sale, involving perhaps washing, crushing and grading or blending according to lump size or composition.

This chapter will concentrate on those aspects of operations (a) and (b) which involve process modelling for the design of controls, the satisfactory performance of which is essential to efficient mining. Coal and mineral preparation processes, (c), tend to be manageable by conventional process control techniques and will therefore not be studied in detail here. It is within the areas of winning and clearance that process models have characteristics which are, at first sight, peculiar to mining and therefore deserving of a special chapter devoted to their development. Important points of contact with process models outside the mining field will also become apparent however thereby hopefully contributing to the art of process modelling generally.

Of course an enormous number of activities are also involved in mining without which the three basic operations (a), (b) or (c) could not take place. These include, for instance, mineral location by exploration and drilling, marketing, mine development, plant maintenance, the supply of services such as electricity, compressed air, men, materials and ventilation to all points in the production network, the removal of water and also unsaleable rock, (necessarily extracted to provide underground roadways of a size adequate for the free flow of product and services

throughout the mine). Indeed every underground process from the hoisting of material from the pit bottom to the supply of power to the many hundreds of machines could fairly be termed a "mining process" in its own right despite the existence of apparently related processes in industry generally. What makes the mining versions special are:

(i) the enormous distances and depths over which the processes operate

(ii) the massive nature of the machines involved to withstand the arduous underground environment which imposes the most severe stresses from heat, rockfall, water and dust and, in coal mining, because of the need for flameproofness of electrical equipment to avoid methane ignition.

and

(iii) the non static nature of mining which must constantly chase a retreating product so necessitating the continual evolution and extension of the back-up systems required for its extraction.

Space does not unfortunately permit investigation of these subsiduary but essential processes.

In mining as in all productive industries, the key dependent variables requiring control are product quality and the rate of production. The attainment of high levels for both simultaneously often imposes a compromise dictated by market factors, costs and safety considerations. In this chapter we shall therefore devote attention to aspects of the winning and clearance operations which crucially affect the quality and quantity of the mineral extracted. The dynamics of cutting will be investigated since this process affects the lump size, and therefore the quality, of the product whilst having an important bearing on the rate of which cutting machines can progress. The steering of these machines through the strata will also receive attention since it is by successful steering that the volume extracted of the desired product can be maximised

without risk of contamination resulting from the accidental cutting of unwanted rock strata above and beneath (or to either side) of the seam (or vein) of the desired mineral. If the seam, or vein, is softer than the surrounding strata then clearly successful steering also assists the increase of bulk production rate.

Some adjustments to product quality can, of course, be made after the initial winning of the product by crushing, separation, and blending etc. either in the product-preparation phase of operations or, at intervals, in the clearance system. The prime purpose of the clearance system is, however, the rapid removal of the product through the mine to the surface without the development of spillage or bottlenecks and the modelling of such systems to achieve this goal by proper control will be examined.

There exists throughout mining a great variety in the types of individual machine and machine systems employed and a comprehensive coverage cannot be accomplished within the confines of a single chapter. The description of only some of the types in merely qualitative terms could easily occupy an entire volume. The aspects considered and the approach to modelling the particular examples, (drawn largely from coal mining), here presented will nevertheless by found to apply in most mining situations. Furthermore, the behavioural characteristics predicted for these specific model examples will also be found to apply, at least qualitatively, to most related mining systems which will differ only in detail, and not in basic principle of operation, from the examples considered.

13.2 The dynamics of coal and mineral cutting

Cutting machines, in principle at least, resemble machine tools designed for the shaping of metals and, despite some important differences such as substantial frictional effects, a good deal can be learned from attempts[1],[2] to model their cutting actions that is useful in predicting

aspects of the behaviour of coal - rock - and mineral-cutting machines. Like machine tools they incorporate two fundamental mechanisms which are:

(i) a cutting head, usually rotary in operation, the cutting picks of which tear material fromthe rock-or coal-face

and,

(ii) a feed- or, in mining terminology, haulage-mechanism provided to advance the cutting head linearly into the solid rock or coal as the previously fractured material is continuously cleared.

To prevent the uncontrolled build-up of cut material around the cutting head, this unit is usually equipped with vanes or paddles which fling the cuttings onto some form of automatically advancing conveyor which, whilst being intimately linked to the cutting machine, may be regarded as the first link in the conveying chain which constitutes the clearance system.

Fig. 13.1 illustrates the cutting action of a shearer or milling machine in which the cutting drum or disc rotates about an axis perpendicular to the direction of feed or haulage whereas a trepanner-head rotates about an axis parallel to the haulage direction as shown in Fig. 13.2. A diagramatic plan view of a shearer machine is shown in Fig. 13.3 which illustrates a machine with an inbuilt laulage system which pulls the machine along a fixed rope or chain as shown. As an alternative an external winch may be used for haulage purposes situated at one or other end of the face. In this case the cutting machine is hauled by a moving loop of chain (or rope) which passes round the powered haulage drive sprocket at one end of the face and an idler sprocket at the other. The stiffness of the haulage system therefore varies with the length of chain or rope in tension which varies from one face length to near zero in the case of inbuilt haulage and from either two to one, or one to near-zero face lengths in the case of external haulage, depending on the side of the loop to which the machine is attached. In either case a chain or rope type of haulage system is far

from stiff for much of the time because of the long lengths of face* which are generally employed. Because of the potential hazard presented by long, highly stretched, ropes and chains, and to avoid control problems posed by their varying stiffness, rack-and-pinion haulages have recently been developed.

Figs. 13.2 and 13.3 also serve to illustrate how, in so called longwall mining the mineral is removed not by a simple forward tunnelling procedure but be repeated passes or sweeps of the cutting machine, exposing a new face with each pass. The machine, and indeed the whole face installation, comprising roof supports, conveyor and services is advanced by hydraulic jacks between successive passes by a distance W_d, generally equal to the width of the cutting drum or disc or the diameter of say a trepanner head to ensure maximum extraction of mineral on each pass. The direction of machine travel, whilst cutting, and the general direction of mineral extraction over a period of several passes, or cuts, are therefore perpendicular to one another, the former being known as the along-face direction and the latter, the face-advance direction. These directions are indicated in Figs. 13.1, 13.2 and 13.3. Provided the cutting machine with its supporting installation is fully advanced between cuts then the multipass nature of the longwall process has little direct bearing on the cutting process as such but has a profound effect on machine steering as will be shown in section 13.3.

13.2.1 Modelling the cutting-head

The rotary cutting-head is fitted, around its periphery, with a number of cutting picks, which are responsible for tearing the coal or mineral from the solid face and which therefore absorb the bulk of the power supplied to the cutting machine through its haulage and cutting-head drive motors. The circumferential forces on these picks are provided by the cutting-head

* A fuller discussion of so called 'longwall' mining will be found in the introduction to section 13.3.

drive whilst the net horizontal force* on the head, arising from the vectorial summation of all the radial pick-force components in the case of a shearer or miller (or the total of the axial force components in the case of a trepanner) is provided by the haulage. Any resultant of the sideways forces on the cutting picks will produce friction forces between the machine and either the face-wall or the floor or track upon which the machine slides which in turn will be overcome by a small proportion of the power available from the head and haulage drive motors.

Now in fundamental laboratory experiments[3],[4],[5] on individual cutting picks it has been shown that all three components of the cutting force depend predominantly on the following factors:

(a) the geometry, general design and sharpness of the pick itself,

(b) the bite, or penetration of the pick into the material,

and

(c) the hardness, H, of the material being cut.

Furthermore, for a given type and sharpness of pick, the force/bite relationship is substantially linear over a wide range of penetrations. For the entire cutting head therefore it may be assumed that the net horizontal (along-face) and circumferential forces $F_h(t)$ and $F_c(t)$ are given by

$$F_h(t) = k_h(H)\ y(t) \tag{13.1}$$

and

$$F_c(t) = k_c(H)\ y(t) \tag{13.2}.$$

where k_h and k_c are machine and mineral constants varying, for a given machine, with the mineral hardness and pick sharpness. The variable $y(t)$ is the effective bite taken by the cutting head.

Now consideration of Fig. 13.2 would indicate that, in the case of a trepanner head, $y(t)$ is governed by the differential equation

$$dy(t)/dt = v_2(t) - v_2(t - T_d) \tag{13.3}$$

where v_2 is the speed of translation of the cutting machine along the face

* More precisely this force should perhaps be described as the net along-face cutting force to allow for inclined seams.

and T_d is the interval between the arrival of consecutive picks, being given by

$$T_d = \Theta_p/\Omega \qquad (13.4)$$

where Θ_p is the angular spacing of the picks and Ω the angular speed of the head. T_d is virtually constant, cutting heads being driven generally by squirrel-cage induction motors. With a miller or shearer type of cutter, as illustrated in Fig. 13.1, y(t) is also given by equation 13.3 but the disc or drum is shown, in the figure, not at a general point but at a particular point in its rotation, viz at the point of maximum bite: even with a constant speed, v_2, the instantaneous bite will clearly vary as the drum rotates, being zero at top and bottom. To merely substitute equation (13.3) into (13.1) and (13.2) to obtain the instantaneous cutting forces is therefore clearly an approximation in the case of shearer and milling machines.

That bite and hardness should be the principal variables affecting cutting forces is clearly reasonable in view of the experimental results for single picks but the analytical generalisation of these findings to the multi-pick, field situation is not completely straightforward, partly for the reasons given above and partly because the leading pick of a group may relieve considerably the load imposed on those immediately following by bursting off a lump larger than its penetration prior to mineral fracture. Groups or lines of picks are therefore often best regarded as single effective picks. A shearer drum for instance, as illustrated in Fig. 13.4, is usually laced with, i, - typically 2 or 3 spiral lines of picks to assist the clearance of the cut material and such a drum is often best regarded conceptually not as a number of miller discs assembled side-by-side with staggered picks, but as a single miller disc having only i - effective picks since the cutting load tends to be concentrated on the face-side of the drum.

Equations 13.1 to 13.3 therefore provide a reasonable conceptual basis for dynamic modelling but care is needed in establishing the number of effective picks, and therefore the effective value of T_d, and in predicting values for k_h and k_c from single-pick data. Confirmatory field experiments clearly play an important role in any novel situation. In the case of the trepanner, least error is involved in the use of equation 13.3. If the object of modelling is however to determine, say, the total torque or power consumption of the cutting head or haulage drive then the necessity for these motors to drive additional jibs and discs to square-off the original cylindrical excavation cut by a trepanner head introduces complications. The effect of the breaker picks (see Fig. 13.2) for shattering the core cut by the head would also require investigation for really rigorous model development. Since these operations tend to consume a relatively small proportion of the available power however, they may be reasonably disregarded in the structure of the conceptual model and accounted for by appropriate increases in the values of parameters k_h and k_c. The values of k_h and k_c are comparable for conventional pick and head designs which means that the ratio of the power ratings for head and haulage drive is dictated largely by the ratio $\Omega.r./\bar{v}_2$, where r is the radius of the cutting head and $\bar{v}_2$ the mean value of $v_2(t)$. Machines such as shearers and trepanners designed to extract deep webs (i.e. large W_d) are generally slow-moving along the face and hence their cutting head drives draw considerably more power than do their haulages, typical machine ratings being 200 and 20 kw respectively. The haulages of fast-traversing millers on the other hand may absorb a considerably larger fraction of the total power used.

13.2.2 Modelling the haulage/transmission system

Because of the resilience of the transmission, the instantaneous translational speed $v_1(t)$ of the haulage/transmission drive may differ considerably from the machine speed $v_2(t)$, particularly in the case of

rope or chain hauled machines. If therefore $\tau(t)$ denotes the tension in the transmission then

$$d\tau(t)/dt = k_a(\ell)\ \{v_1(t) - v_2(t)\} \qquad (13.5)$$

where k_a is the stretch modulus of the transmission which, as indicated in equation 13.5 will be dependent upon the length, ℓ, of rope or chain in tension, in such a system. Generally the average speed of haulage is sufficiently small for any change in ℓ to be negligible within the settling time or oscillation period of the slowest system mode so permitting dynamic simulations to be carried out at constant values of k_a pertaining to various points along the face. In the case of stiff transmissions exhibiting negligible deviation between v_2 and the speed of the final drive member, some resilience between v_2 and the set speed of the drive will generally occur nevertheless due usually to the compressibility of hydraulic fluid. Interpreting v_1 so the set speed in such situations therefore permits the use of equation 13.5, k_a now being position-invariant and related to the stiffness of the haulage drive itself.

The tractive effort $\tau(t)$ applied by the haulage/transmission to the cutting machine must provide not only the total resolved along-face cutting force $F_h(t)$ but must also overcome static and sliding frictional forces between the machine body or skids and the conveyor track or rough floor upon which the machine slides. Any linear acceleration forces required must also be provided by $\tau(t)$. We therefore have the force balance equation

$$\tau(t) = F_h(t) + F_f(t) + M\ dv_2/dt \qquad (13.6)$$

where $F_f(t)$ is the frictional force given by

$$F_f(t) = \{\text{signum } v_2(t)\}\ F_s, \quad |v_2(t)| > 0 \qquad (13.7)$$

and

$$F_f(t) = \tau(t) - F_h(t),\ v_2 = 0 \text{ and } |\tau(t) - F_h(t)| < F_b \qquad (13.8)$$

where F_s and F_b are the values of sliding and static frictional forces respectively, F_b being greater than F_s and both positive. The parameter M

is the mass of the machine lumped together with one third that of the rope or chain, the frequencies of disturbances transmitted along the rope or chain not usually being high enough to warrant the use of a distributed mass/elasticity model.

13.2.3 Modelling the cutting head drive

Except in the case of high speed millers where haulage power may exceed disc power, it is generally necessary to regulate the power or current consumption of the cutting-head drive, (the power rating of which lies generally in the range 100 to 400 kw), by manipulation of the adjustable haulage drive speed $v_1(t)$ as the hardness H of the coal, rock or mineral varies. This drive is usually a squirrel cage induction motor of substantially constant speed as has already been mentioned but exhibiting some speed droop with increase in load nevertheless. Whilst insufficient to seriously affect the value of T_d (Section 13.2.1), in conjunction with the inertia of the drive motor, the speed droop does give rise to a significant time-constant T_m in the response $P_e(t)$, the electrical power drawn by the motor, to disturbance $P_m(t)$, the mechanical power delivered to the cutting head. Within the normal working speed range of the motor we therefore have that

$$T_m \, dP_e(t)/dt = k_e \, P_m(t) - P_e(t) \qquad (13.9)$$

where k_e, (> 1), is a parameter related to the drive efficiency which may be assumed constant over the normal load range. The mechanical power $P_m(t)$ may in turn be related to the net circumferential cutting force $F_c(t)$ thus

$$P_m(t) = k_d \, F_c(t) \qquad (13.10)$$

where k_d is a machine parameter which, whilst depending on rotational speed Ω, may again be taken as constant in studies of perturbations around normal load conditions.

13.2.4 The overall system model behaviour

By taking Laplace transforms, in s with respect to t, of the foregoing differential equations and assembling all the resulting algebraic equations, a block diagram of the composite system may be readily derived. Such a

diagram is shown in Fig. 13.5 which also includes the representation of a closed-loop controller for the regulation of $P_e(t)$ to a reference value $P_{ref.}$ As indicated, measurement of P_e usually involves the smoothing action of a low-pass filter, time constant T_e, to remove the alternating component of P_e and an actuator lag T_h is also involved in the manipulation of the set speed $v_1(t)$. The controller shown has a gain K and is of the pure integral type in accordance with usual practice. In Fig. 13.5, the non-linear relationship between machine speed v_2 and net applied force $\tau - F_h$ is represented by the describing function G_F/Ms which will be discussed later in connection with analytical predictions of system behaviour. For the moment we shall devote attention to computed solutions obtained directly from equations 13.1 to 13.10.

The system's open-loop response to a step change in $v_1(t)$, at constant H, first reported[6] by the author in 1978 along with much of the material of Section 13.2 is shown in Fig. 13.6 for the following realistic system parameters

$v_1(t)$ = 0.0762 m/s, increasing to 0.1270 m/s

k_a = 12700 kg/m ($\equiv \ell$ = 300m)

$k_c = k_h$ = 68800 kg/m

T_d = 0.4 s

F_s = 2270 kg

F_b = 4540 kg

M = 5120 kg

From the Fig. 13.6 it is clear that, in the presence of the cutting force F_h, the behaviour of v_2 is very different to that which would be expected if v_2 were restrained by friction and inertia alone. Under such circumstances it would be expected that for changes in $v_1 << v_{2max}$, the size and shape of the v_2 - pulse should be little affected by the change in v_1 and the change should result instead in a change in the frequency of hopping. Indeed the value of v_{2max} in the absence of F_h would be

approximately $(F_b - F_s)/(k_a M)^{0.5} = 0.88$ m/s for the given parameters, compared to the much smaller values of Fig. 13.6 The increase in v_1 in fact causes only a marginal increase in frequency but produces a substantial change in v_{2max} as shown. The frequency f of hopping always lies in the range,

$$0.5T_d^{-1} < f < T_d^{-1} \qquad (13.11)$$

and is therefore dictated by drum rotation rather than mere stick/slip phenomena which would produce a wide variation in the frequency of hopping with changing v_1. This hopping at near effective-pick frequency is a well known characteristic of real machines and therefore its prediction provides a good measure of confidence in the model.

It is important also to notice that the tension τ varies little in the presence of F_h whereas it would undergo wild fluctuations in the presence of friction alone. By contrast, the hopping, or chatter - to use the analogous term in machine-tool dynamics, exhibited by v_2 is strongly manifested in the F_c-, and therefore the P_m- trace, with important practical implications since stall values are easily attained if the mean value of P_e is regulated close to the continuously rated value* for the motor.

Load oscillations are in fact made worse by the addition of a responsive integral controller as predicted by Fig. 13.7 which is obtained from the simulation of the identical machine as for Fig. 13.6, with cutting head drive and control system parameters as follows:

v_{1max} = 0.203 m/s

K = 0.0051 m/s/kw

k_d = 0.0355 kw/kg

* Typically the stall value of P_e = 2 to 2.5 times the continous rating of an induction motor.

$k_e = 1.25$

$T_m = 0.05s$

$T_e = T_h = 0.10s$

Low-frequency limit-cycling of the control system is now superimposed on all traces to varying degrees and clearly accentuates the problem of stalling. By way of confirmation, Fig. 13.8 shows an actual field trial recording of P_e obtained on the same shearer machine as that for which the foregoing parameters were estimated. The high- and low-frequency components are clearly comparable in amplitude and frequency with those predicted and it was found necessary in practice to reduce P_{ref} to about 75% of the rated value of P_e to avoid regular stalling of the motor and the consequent loss of production and risk of motor burn-out through restarting too frequently.

13.2.5 Analytical Predictions.

Whereas the simulation experiments for particular cases seem to accord with field experience it is also important to be able to make at last approximate predictions of system behaviour from the theoretical model without recourse to computer simulation if only to restrict the number of simulation experiments otherwise necessary to obtain a comprehensive picture of system performance under a wide range of load conditions and parameter values. It is in the frequency domain that such analytical solutions are generally most readily obtained (see chapter 2), so requiring a model formulated in terms of interconnected transfer-functions as Fig. 13.5. Unfortunately the frictional effects described by equations 13.7 and 13.8 are highly nonlinear so that the operator $G_F(s)$ shown in Fig. 13.5 relating the net applied force F_a,$(= \tau - F_h)$ to the acceleration force $M\,dv_2/dt$ will be highly dependent upon its input signal amplitude $\hat{F}_a$ so that G_F is properly denoted as $G_F(\hat{F}_a, s)$. Of course $G_F(\hat{F}_a, s)$ strictly describes only the effect of the frictional process on the fundamental component of an oscillating input

signal of non sinusoidal wave shape and the ommission of parallel transfer-functions processing any higher frequency harmonics is justified only if it can be assumed that these are effectively attenuated in passing round the feedback loops containing the nonlinear operation. The integration process $1/Ms$ immediately following the so called describing function $G_F(\hat{F}_a,s)$ in Fig. 13.5 should certainly aid the attenuation of harmonics in this case. Before proceeding therefore it is necessary to determine the nature of G_F by considering a sinusoidal force $\hat{F}_a \sin \omega t$ applied to the friction restrained machine.

13.2.5.1 An approximate describing-function representation of friction

Fig. 13.9 illustrates the response $v_2(t)$ of a machine subject to a sinusoidal force $F_a(t) = \hat{F}_a \sin \omega t$ and restrained by static and sliding friction described by equations 13.7 and 13.8. As indicated the motion will be discontinuous if $\hat{F}_a$ is small enough to ensure that the angle θ_b of breakaway and the angle θ_s at which the machine again becomes stationary are separated by less than half a half cycle of oscillation, i.e.

$$\theta_s < \pi + \theta_b \tag{13.12}$$

For any motion to take place of course we must have that

$$\hat{F}_a > F_b \tag{13.13}$$

Now θ_b is given by

$$\theta_b = \sin^{-1}(F_b/\hat{F}_a) \quad , \quad o < \theta_b < \pi/2 \tag{13.14}$$

and θ_s can be obtained by integrating the equation of motion, viz

$$M dv_2/dt = \hat{F}_a \sin \omega t - F_s \ , \quad \theta_b < \omega t < \theta_s \tag{13.15}$$

and setting $v_2(t)$ to zero so that

$$(F_s/\hat{F}_a)(\theta_s - \theta_b) = \cos \theta_b - \cos \theta_s \tag{13.16}$$

Now maximum velocity $\hat{v}_2$ will occur when $\omega t = \theta_m$ where

$$\theta_m = \pi - \sin^{-1} (F_s/\hat{F}_a) \tag{13.17}$$

and, since integration of the equation of motion, (13.15), gives

$$v_2(t)\ \omega\ M = \hat{F}_a(\cos\ \theta_b - \cos\ \theta) + F_s(\theta_b - \theta) \tag{13.18}$$

where $\theta = \omega t$ (13.19)

on substituting θ_m for θ we get, using equation 13.14 and 13.17,

$$\hat{v}_2\ \omega\ M/\hat{F}_a = \{1 - (F_s/\hat{F}_a)^2\}^{0.5} + \{1 - (1 - F_b/\hat{F}_a)^2\}^{0.5}$$

$$+ (F_s/\hat{F}_a)\ \{\sin^{-1}(F_s/\hat{F}_a) + \sin^{-1}(F_b/\hat{F}_a) - \pi\} \tag{13.20}$$

so yielding an expression for the velocity amplitude in terms of the applied force parameters $\hat{F}_a$, ω and system parameters. Turning attention to the relative phase of the force and velocity oscillations, it is clear that the angle, ϕ, by which $\hat{v}_2$ lags $\hat{F}_a$ is, from inspection of Fig. 13.9 equal to $\theta_m - \pi/2$ so that, from equation 13.17

$$\phi = \cos^{-1}(F_s/\hat{F}_a) \tag{13.21}$$

Now equations 13.20 and 13.21 permit the calculation of the peak value of the actual (or total) v_2 waveform and its phase-displacement from the peak of the applied force wave-form F_a whereas it is the amplitude and phase shift of the fundamental component of $v_2(t)$ which is strictly required to determine the describing-function $G_F(\hat{F}_a,s)$. As already mentioned however, the describing-function approach is itself approximate through its neglect of harmonics and it is therefore reasonable to regard the vector $(\hat{v}_2/\hat{F}_a), \angle\phi$ as a close approxmation to the desired transfer-function $\{G_F(\hat{F}_a,j\omega)\}/\{j\ \omega\ M\}$ We therefore have that

$$G_F(\hat{F}_a\ ,\ j\omega) \simeq (\hat{v}_2\ \omega\ M/\hat{F}_a)\ ,\ \angle(\phi - \pi/2) \tag{13.22}$$

the modulus being obtainable from equation (13.20) and the argument from (13.21). From these equations it is immediately obvious that neither of these two coordinates is frequency dependent, the right hand sides being functions only of amplitude $\hat{F}_a$ and the friction parameters F_s and F_b so permitting the argument $j\omega$ to be dropped from the function G_F , i.e.

$$G_F = G_F(\hat{F}_a) \tag{13.23}$$

For given F_s and F_b values therefore a single locus, with $\hat{F}_a$ as parameter, of G_F may be calculated and drawn in polar form, but only for the range of $\hat{F}_a$ for which discontinuous oscilllation occurs, i.e. for which equation (13.12) holds. Substituting equations (13.14) and (13.16) yields the upper bound for $\hat{F}_a$, given by

$$\hat{F}_a/F_b < \{1 + (\pi\alpha/2)^2\}^{0.5} \tag{13.24}$$

where $$\alpha = F_s/F_b \tag{13.25}$$

Above this bound, F_a produces a continuous response as sketched in Fig. 13.10, the motion and the fictional force changing sign at angles θ_o and $\theta_o + \pi$ from the commencement of the force cycle. Integrating the equations of motion between these limits gives:

$$\theta_o = \cos^{-1}\{(F_s/\hat{F}_a)(\pi/2)\} \tag{13.26}$$

the necessary condition that $\hat{F}_a/F_s > \pi/2$ being always met since motion will occur in practice if

$$\hat{F}_a/F_s < \{(\pi/2)^2 + (1/\alpha)^2\}^{0.5} \quad ; \ (> \ \pi/2)$$

as may be derived from constraint (13.24).

The expressions for θ_m and ϕ (13.17) and (13.21) remain unchanged for continuous motion so that the phase of $G_F(\hat{F}_a)$ is also unaltered. The peak velocity $\hat{v}_2$ is now governed by an expression different to that of equation (13.20) however, since on integrating the equation of motion we now get

$$\hat{v}_2 \ \omega \ M = \hat{F}_a(\cos\theta_o - \cos\theta) + F_s(\theta_o - \theta)$$

and on eliminating θ_o, using (13.26) and substituting for θ_m using equation (13.17) we get

$$\hat{v}_2 \ \omega \ M/\hat{F}_a = \{1 - (F_s/\hat{F}_a)^2\}^{0.5} + (F_s/\hat{F}_a)\left[\cos^{-1}\{(F_s/\hat{F}_a)(\pi/2)\} + \sin^{-1}(F_s/\hat{F}_a) - \pi/2\right] \tag{13.27}$$

and, under these conditions equation (13.27) is the one from which $|G_F(\hat{F}_a)|$ should be calculated.

Fig. 13.11 illustrates the resulting form of the loci of $-G_F(\hat{F}_a)$ which clearly changes for different ratios α of sliding to static friction as shown. The lower boundary of the loci is however independent of α as would be expected since this portion of the locus derived from equation (13.27), represents continuous motion which is obviously unaffected by F_b. The calibration of the individual locus brances is given in Table I.

Table I. Values of $\hat{F}_a/F_s$ pertaining to points plotted in Fig. 13.11

α	Point No.							
	1	2	3	4	5	6	7	8
0.25	4.00	4.12	4.20					
0.40	2.50	2.75	2.95					
0.50	2.00	2.10	2.20	2.30	2.40	2.50		
0.60	1.67	1.83	2.00	2.15	2.28			
0.75	1.33	1.47	1.60	1.73	1.87	2.05		
1.00	1.00	1.11	1.25	1.33	1.50	1.70	1.75	1.86

13.2.5.2. Prediction of chatter

Between the two points A and B marked on the system block diagram of Fig. 13.5 there are effectively two transfer-functions arranged in a negative feedback configuration as illustrated in Fig. 13.12. The forward path transfer-function is the frequency-independent describing-function $G_F(\hat{F}_a)$ already determined, whilst the feedback transfer-function $G_1(s)$ is derived by reducing the network of series and parallel transfer-functions connected around the two points A and B, and describing the remainder of the system. Limit-cycling will clearly occur at a frequency ω and applied-force amplitude $\hat{F}_a$ at which

$$G_1(j\omega)\ G_F(\hat{F}_a) = -1.0$$

i.e., when

$$G_1^{-1}(j\omega) = -\ G_F(\hat{F}_a) \qquad (13.28)$$

where the inverse Nyquist locus of $G_1(s)$ intersects the locus of $-G_F(\hat{F}_a)$. The advantage of having isolated $G_F(\hat{F}_a)$ in its present form is that the effect of varying all the system parameters (other than F_s and F_b) may be investigated by redrawing only the locus of $G_1^{-1}(s)$, $G_F(\hat{F}_a)$ remaining unchanged.

With the automatic control loop open, $G_1^{-1}(s)$ is readily shown to be given by

$$G_1^{-1}(s) = M\, s^2 / [k_a + k_h \{1 - \exp(-T_d s)\}] \qquad (13.29)$$

the locus of $G_1^{-1}(j\omega)$ clearly oscillating in phase between the limits $\pi \pm \gamma$, where

$$\gamma = \sin^{-1}\{k_h/(k_a + k_h)\} \qquad (13.30)$$

and crossing the real axis at distances x, where

$$x = -\frac{(n\pi)^2 M}{T_d^2 (2 k_h + k_a)} \quad , n = 1,3,5$$

and (13.31)

$$x = -\frac{(n\pi)^2 M}{T_d^2 k_a} \quad , n = 0,2,4$$

at frequencies $\omega = n\pi/T_d$, n = 1,2,3 (13.32)

as illustrated in Fig. 13.13.

The ratio k_a/k_h of the stiffnesses of the transmission and cutting loops is clearly an important parameter in dictating the frequency of any limit cycling which must, from observation of the loci $G_1^{-1}(j\omega)$ and $-G_F(\hat{F}_a)$ for the system of Section 13.2.4 shown in Fig. 13.14, clearly occur in the range

$$\pi\, T_d^{-1} < \omega < 2\, \pi\, T_d^{-1} \qquad (13.33)$$

for $k_a/k_h << 1.0$* for machines of large mass M: as we have already observed in the simulation of this system. Values of ω, $\hat{F}_a$ and $\hat{v}_2$ determined from the intersection of $G_1^{-1}(j\omega)$ and $-G_F(\hat{F}_a)$ are also found to accord well with simulation. Increasing the stiffness of transmission above k_h clearly begins to reduce γ and compress the oscillation of the

* The minor role played by the transmission under these circumstances is confirmed by the small proportion of ripple exhibited by tension, Υ, in Fig. 13.6.

$G_1^{-1}(j\omega)$ locus about the negative real axis by moving the frequency of intersection towards the limiting value $\sqrt{k_a/M}$ so that chatter is then dictated by transmission resonance rather than cutting head dynamics. This prediction is likewise confirmed by simulation.

The incorporation of the control loop dynamics into $G_1(s)$ has but a minor effect on the locus shape in the vicinity of its intersection with $-G_F(\hat{F}_a)$, provided the gain K is relatively small so that control action can do little under such circumstances to combat high frequency chatter. The low frequency behaviour of the automatic control loop is considered in the following section of this chapter.

13.2.5.3. Prediction of low-frequency behaviour

For the purposes of low-frequency servo design the dynamics of the cutting loop (1) in Fig. 13.5 may be drastically simplified. Static and sliding frictional effects are ignored altogether making $G_F = 1.0$ and the regenerative cutting dynamics

$$\tilde{y}(s)/\tilde{v}_2(s) = \{1 - \exp(-T_d s)\}/s \qquad (13.34)$$

{obtained by taking Laplace transforms of equation (13.3)}

approximated by expanding the R.H.S. of (13.34) and ignoring powers of s above the first so that

$$\tilde{y}(s)/\tilde{v}(s) \simeq T_d/(1 + 0.5\, T_d s) \quad , \quad |T_d\, s| << 1.0 \qquad (13.35)$$

As an alternative approach, recalling that the use of (13.3) is itself an approximation, the cutting dynamics may be modelled, for low-frequency effects only, by imagining the coal or mineral buttock wall to move forward not in discrete slices but at a continuous velocity $v_b(t)$ as it is attacked by the drum moving with a linear velocity $v_2(t)$. Fig. 13.15 illustrates this concept. Only in steady-state will v_b and v_2 reach equality and under transient conditions the differential equation

$$dy(t)/dt = v_2(t) - v_b(t) \qquad (13.36)$$

will apply. Now $v_b(t)$ is the rate at which material is torn from the

buttock and therefore

$$v_b(t) = y(t)/T_d \tag{13.37}$$

so that elimination of $v_b(t)$ between (13.36) and (13.37) produces the result:

$$\tilde{y}(s)/\tilde{v}_2(s) \simeq T_d/(1 + T_d s) \tag{13.38}$$

The two approaches clearly produce first-order lag models for the cutting dynamics but having time-constants of different magnitude. These are fortunately significantly smaller than the dominant system lags so that the resulting differences in the predicted behaviour of the complete system are only marginal.

Ignoring friction, equation (13.6) becomes

$$\tau(t) = F_h(t) + Mdv_2(t)/dt = k_h\, y(t) + Mdv_2(t)/dt \tag{13.39}$$

and with this simplification and that of equation say, (13.35) the transfer-function of the open control loop becomes

$$G(s) = \frac{K\, k_c\, k_d\, k_e\, T_d}{s\{1 + T(1-0.5T_d s)s - (0.5T_d s^2/\omega_o^2)\}(1 + 0.5T_d s)(1 + T_m s)(1 + T_e s)(1 + T_h s)} \tag{13.40}$$

$$\text{where } T = T_d\, k_h/k_a \tag{13.41}$$

$$\text{and } \omega_o = (k_a/M)^{0.5} \tag{13.42}$$

Now for highly elastic transmission $T >> T_d$ and provided the resulting model predictions are confined to frequencies much less than $1/(0.5\, T_d)$ and ω_o (= 5 and 4.93 rad/s in the example considered) G(s) may be simplified to a cascade of first-order lags, thus:

$$G(s) \simeq \frac{K\, k_c\, k_d\, k_e\, T_d}{s(1 + T\, s)(1 + 0.5\, T_d s)(1 + T_e\, s)(1 + T_h s)(1 + T_m s)} \tag{13.43}$$

$$= 12.4/\{s(1 + 2.17\, s)(1 + 0.2\, s)(1 + 0.1\, s)^2(1 + 0.05\, s)\} \tag{13.44}$$

in the particular example considered earlier.

The open-loop $v_2(t)$ trace of Fig. 13.6 clearly shows a near exponential envelope having a time-constant very similar to the 2.17 s predicted by

(13.44). The inverse Nyquist locus of G(s) shown in Fig. 13.16 indicates a critical frequency of 0.97 rad/s (0.154 Hz) which is consistent with the simulated and observed frequencies of servo oscillation (0.120 and 0.128 Hz respectively) shown in Figs. 13.7 and 13.8. Had a lag of time-constant T_d(= 0.4s), rather than 0.5 T_d been used in the calculation of G(s) then agreement would have been even closer suggesting that the continuous cutting action concept is perhaps marginally superior to the discrete bite concept for modelling of the cutting process in the low-frequency domain. Such a low-frequency model was indeed employed[7] long before the incorporation of detailed cutting-loop effects for the design of stable load controllers which eliminate the low-frequency oscillations exhibited by Figs. 13.7 and 13.8. The value of the detailed model lies, of course, in its potential to aid the elimination of chatter either by adjustments to machine design or by responsive regulator action.

13.3 Steering dynamics

We now turn attention from the process of cutting, as such, to the associated and equally important process of steering the cutting machine. Whilst cutting dynamics affect predominantly the rate of mineral extraction, steering dynamics affect the composition of the product if, in the interests of productivity, the size of the cutting head is close the the seam thickness. Good steering is, in any event, an essential prerequisite to safe and effective mining yet its satisfactory control is far from simple.

13.3.1. Fundamental features

A winning machine will not follow automatically the seam or vein of desired material unless means are provided

(a) to deflect the direction of the cutting head in the two directions perpendicular to its line of travel

(b) to detect any deviation of the cutting head outside the boundaries of the desired material and into the unwanted surrounding strata, and

(c) to interlink operations (a) and (b), above, by a suitable control strategy.

As in most physical steering processes operating in a terrestrial, marine or aerial environment, the steering mechanism, (a), effects a change in the angle of attack of the machine itself. At their simplest therefore, the steering dynamics involve two cascaded integrations* between the deflection of the steering actuator, (generally hydraulic in mining applications), and the resulting position of the machine in space. Furthermore, the error-sensing operation, (b), usually involves some transport-delay because of the obvious engineering difficulty, (if not impossibility), of siting a sensor at the point of cutting. Human observation of the position of the cutting head is restricted likewise because of the dense dust cloud created in its immediate vicinity.

Sensor and actuator dynamics are often significant in steering control, particularly the former because of the random nature of the low-power radiation techniques[8][9], often employed to detect the difference in strata characteristics. In some instances the alternative technique of monitoring the variation in cutting force is employed as a means of detecting movement of the cutting head outside the desired stratum but, because of the very random nature of the measurements, considerable delay and filter dynamics may be involved in producing the desired positional information.

These factors constitute the fundamental ingredients of the steering dynamics of tunnelling-type systems, i.e. those mining systems in which the direction of machine travel - whilst cutting, and the general direction of mineral extraction are colinear. The modelling and control problems for steering such systems, whilst being far from trivial are comparatively straightforward. However, with longwall mining, (which is by far the most common method of underground coal extraction in Europe - and increasingly

* Integrations with respect to distance traversed in the general direction of cutting.

popular in North America), serious additional complications are introduced requiring very careful consideration. These are now examined:

13.3.2 Geometrical modelling of a longwall system

Fig. 13.17. shows diagramatically those features and variables of a modern longwall shearer machine (and the associated mechanical system) essential to the modelling of its vertical steering characteristics. The machine makes repeated sweeps, or passes, along the coal face of length, L, extracting on each pass a volume of material = L W_d D, where W_d and D are the drum width and diameter respectively: assuming perfect horizontal steering*. As indicated, the machine rides on the semi-flexible structure of an armoured face conveyor (a.f.c) of the scraper-chain type, and the cutting drum may be ranged up and down continuously in an attempt to keep the drum within the boundaries of the undulating coal seam.

Also as shown in Fig. 13.17, in a process normally termed the pushover, the a.f.c. structure is snaked forward horizontally onto the newly cut floor between passes, its front edge taking up a profile, in the vertical plane, similar to that of the cut floor alongside the new face. In this way, on pushover, the a.f.c. undergoes a tilt-change, at any point along its length (and in the face-advance direction), dependent upon the deflection, J, previously applied to the steering boom in the vicinity of the point in question. The tilt-change results from the fact that the width, W_c of the conveyor trays, or pans, is invariably greater than that of the drum, i.e.

$$W_c > W_d$$

Fig. 13.18 illustrates in end-elevation the tilting of the conveyor brought about by steering action.

The relationships of primary importance in modelling the steering system are basically geometrical involving variable heights and tilts which are, at first sight, function of two independent variables: n, the pass number

* i.e. assuming that the drum is fully embedded to a depth W_d in the coal face on each pass. Horizontal steering is briefly considered in section 13.3.5.

and ℓ, the distance travelled along the face. In the interests of simplicity we shall consider the special case of nearly-equal drum and conveyor widths, viz:

$$W_c = W_d + \varepsilon \tag{13.45}$$

the positive distance, ε, whilst ensuring the tilt-change effect on pushover being small enough to permit the approximation

$$W_c \simeq W_d = W \tag{13.46}$$

in developing the geometrical model. On this assumption, mere inspection of the side-and end-elevations of Figs. 13.17 and 13.18 reveals that, for small angular changes, the following relationships exist between the heights and tilts of the cut-floor, seam and conveyor:

$$y(n,\ell) + z(n,\ell) = h(n, \ell + R) + W\,\alpha(n,\ell + R) + R\,\beta(n, \ell + R) + J(n,\ell) \tag{13.47}$$

$$\alpha(n,\ell) = \{h(n,\ell) - h(n-1,\ell)\}/W \tag{13.48}$$

and

$$\beta(n,\ell) = \{h(n,\ell) - h(n, \ell + F)\}/F \tag{13.49}$$

where $y(n,\ell) + z(n,\ell)$ is the height of the cut floor at the new face wall, $h(n,\ell)$, that of the conveyor's front edge, $h(n-1,\ell)$ that of the rear edge, $z(n,\ell)$, the height of the lower coal-stone interface and $J(n,\ell)$, the linear deflection of the steering boom from its null position. $\alpha(n,\ell)$ and $\beta(n,\ell)$ denote (in radians) the face-advance and along-face tilts of the machine respectively and are calculated on the assumtion that the three skids A,B and C (Fig. 13.17) are in permanent contact with the a.f.c. The system parameters R and F denote the fixed offset distances between the drum and rear skids and between front and rear skids respetively. Equations of somewhat greater complexity could clearly be developed for the more general situation of unequal drum and conveyor widths.

Equation (13.47) to (13.49), in conjunction with some control law for the manipulation of $J(n,\ell)$, would permit the simulation of a single pass of the machine given profiles for $z(n,\ell)$, $h(n,\ell)$ and $h(n-1,\ell)$, but the multipass

solution for $y(n,\ell)$, $n = 1,2,3...$etc., would require, in addition, a model of the pushover and conveyor fitting process relating the next conveyor heights, $h(n+1,\ell)$ and $h(n,\ell)$ to the newly produced floor profile $y(n,\ell) + z(n,\ell)$ and the previous floor $y(n-1,\ell) + z(n-1,\ell)$. The simplest form of model, here termed the rubber conveyor model, assumes complete flexibility of the structure such that, again assuming $W_c \simeq W_d$,

$$h(n+1,\ell) = y(n,\ell) + z(n,\ell) \qquad (13.50)$$

Such a model is idealised in the sense that it is the simplest model possible and reflects the conveyor designers' objective, namely flexibility, ideally. Unfortunately, as we shall see, the system behaviour, as predicted by this model, is far from ideal in the conventional sense of the word. The modelling of the a.f.c's partial rigidity is considered in Sections 13.3.3 and 13.3.4

13.3.2 Simulated performance of system with rubber conveyor model

Using conventional analogue two-term feedback control based on measurements of machine tilt and delayed floor-coal thickness* according to the law

$$J_d(n,\ell) = - k_h y_m(n,\ell) - k_g W \alpha(n, \ell + R) \qquad (13.51)$$

where k_h is the height-gain and k_g the tilt-(orderivative height-)gain, of the controller and J_d is the demanded boom deflection then, in presence of first-order sensor and actuator dynamics of distant constant† X_1 and X_2

* In practice roof - rather than floor - coal thickness is generally the more convenient measurement and the more crucial variable to control since roof stone penetration can lead to serious roof collapse in many instances. With seams of nearly constant thickness the mathematical problem is little affected but double drum machines, one for roof control and one for floor control, may be used in the event of a widely varying seam thickness (or in very thick seams) so posing a two-input, two-output modelling and control problem. This has been examined by Edwards and Greenberg([11]).

† Assuming a constant machine speed v_2, the time constants of the coal sensor and steering actuator are readily converted to the distance base of the steering problem.

respectively, viz:

$$\partial y_m(n,\ell)/\partial \ell = (1/X_1)\{y(n,\ell - X) - y_m(n,\ell)\} \quad (13.52)$$

and $$\partial J(n,\ell)/\partial \ell = (1/X_2)\{J_d(n,\ell) - J(n,\ell)\} \quad (13.53)$$

a response typified by Fig. 13.19 is predicted by model equations (13.47) to (13.53). The predicted system behaviour is clearly totally unstable. This particular result is produced by a system having the parameters $k_h = 0.8$, $k_g = 1.0$, $X = 1.25m$, $X_1 = 0.6m$, $X_2 = 0.165m$ and $R = 0$ The setting of $R = 0$ implies a so called fixed-drum machine in which there is no relative vertical movement between the machine body and drum, which is located above the rear skids, steering being accomplished by raising and lowering of the whole machine body in a pitching or sometimes rolling motion relative to the a.f.c. Making $R > 0$ only worsens the stability problem and no adjustment of the system parameters in the above model will achieve stability short of making $X = 0$ which has proved physically impossible with conventional radiation transducers. Stability can however be achieved by adopting a control strategy based on coal thickness data collected on the previous pass and stored within a computer for nearly one pass length, $L - X$, before being applied to the controller. Equation (13.52) is thus replaced by

$$\partial y_m(n,\ell)/\partial \ell = (1/X_1)\{y(n-1,\ell) - y_m(n,\ell)\} \quad (13.54)$$

This predicted need to develop computer control - an enormously expensive undertaking for the underground environment, clearly makes worthwhile a much more detailed examination of the a.f.c's response to an undulating cut floor, in the hope that its limited flexibility might provide a sufficiently powerful stabilising influence to permit the use of cheap analogue control. The problem is as yet unsolved because the physics involved is complex and the consequences of error due to oversimplification would be enormously costly. A number of simplistic approaches have been tried yielding inconclusive results but a very rational approach outlined in the next section holds promise of a reliable solution.

13.3.3 Modelling of the semi-flexible conveyor

As indicated in Figs. 13.17 and 13.18, the structure of the a.f.c. comprises a chain of steel trays loosely joined end to end. The conveyor is semi-rigid in several senses, viz:

(a), the side-channels of each tray are very stiff

(b), the deck-plate of each tray is fairly stiff

(c), free angular movement between successive trays is hard - limited, in the along-face direction, to $\pm\Delta\gamma$ and,

(d), in the face-advance direction, to $\pm\Delta\alpha$

where $\Delta\gamma$ and $\Delta\alpha$ are constants. Over and above these considerations are the facts that the joints will exhibit some elasticity and the cut floor may undergo some degradation (e.g. planing off of high spots and filling of hollows with fine material) during the pushover phase. Furthermore, being fairly light compared to the machine weight, the a.f.c structure may not remain completely stationary as the machine passes over.

Because of this complexity there exists a strong temptation to fit some simplified model of pre-assumed structure, perhaps using carefully scaled physical models[12] in the first instance for parameter estimation. Such a mathematical model is suggested in Section 13.3.4.3 but for the moment we attempt the rigorous inclusion of at least some of the above-mentioned factors in a derived - (rather than a guessed-) model and assess its potential for enhancement.

To demonstrate the principle of the method with minimal complication we shall in fact include only factors (a) and (c) (above) and disregard (b) (d) and the secondary effects initially. The deck plates are therefore imagined to remain completely flexible (as in the rubber conveyor concept) whilst the side channels are rigidised. The problem therefore reduces to fitting two independent chains of loosely joined stiff rods to two separate undulating line profiles beneath them. Each chain and line may therefore be

treated independently. Fig. 13.20 illustrates the problem variables involved, the along-face axis having been subdivided into I pan-lengths, X_p, and h(i) denoting the height of the left-hand end of rod i counted from the right-hand end of the face. In terms of the earlier notation therefore, but dropping the pass number n,

$$h(i) \equiv h(L - iX_p) \quad , \quad i = 0, 1, 2 \ldots I \tag{13.55}$$

where $$I = L/X_p \tag{13.56}$$

Assuming small angles, the heights of successive joints are clearly related thus:

$$h(i-1) = h(i) + X_p \gamma(i) \tag{13.57}$$

and intermediate heights are given by

$$h(\ell) = h(i) + (\ell - L + i X_p)\gamma(i) \quad , \quad L - iX_p < \ell < L - (i-1)X_p \tag{13.58}$$

Now in the absence of elastic bending, the a.f.c will settle on the undulating cut floor such that its total potential energy E_I is a minimum subject to the two constraints

$$h(\ell) \geq y(\ell) \quad , \quad 0 < \ell < L \tag{13.59}$$

and $$|\gamma(i) - \gamma(i-1)| \leq \Delta\gamma \quad , \quad i = 2,3,\ldots I \tag{13.60}$$

The potential energy δE_i of rod i is given by

$$\delta E_i = mg\{h(i) + h(i-1)\}/2 \quad , \quad i = 1,2,\ldots I \tag{13.61}$$

where 2mg is the weight of the pan, or from (13.61) and (13.57)

$$\delta E_i = mg\{h(i) + X_p \gamma(i)/2\} \quad , \quad i = 1,2,\ldots I \tag{13.62}$$

and the total potential energy if pans 1 to i inclusive is obviously:

$$E_i = \sum_{j=1}^{i} \delta E_j$$

Now we may regard h(i) as a <u>state variable</u> and $\gamma(i)$ as an adjustable <u>control variable</u> in an optimal control problem requiring the minimisation of E_I with respect to the sequence of controls $\gamma(1)$, $\gamma(2)$ ... $\gamma(I)$, subject to the above conveyor equations and constraints. The modelling problem has thus been conceptually transformed into a optimal control

problem† to which the principle of General Dynamic Programming[13] is admirably suited for its solution. This principle translates the original multistage decision process, (in this case the minimisation of E_i with respect to the sequence $\gamma(1), \gamma(2) \ldots \gamma(i)$) into i single-stage decision processes: in this case the minimisation of E_i with respect to $\gamma(i)$ only, given the minimum total energy E^*_{i-1} of pans 1 to i - 1 as a function of h(i-1). For this application the principle may be expressed thus:

$$E^*_i\{h(i)\} = \min_{\gamma(1),\,\gamma(2),\ldots\,\gamma(i)} \left[E_i\{h(i), \gamma(1),\ldots\gamma(i)\}\right]$$

$$= \min_{\gamma(i)} \left[\delta E_i\{h(i), \gamma(i)\} + E^*_{i-1}\{h(i-1)\}\right] \qquad (13.63)$$

Fig. 13.21 flowcharts the computational procedure implied by equation (13.63): Basically, having chosen some arbitrary initial height h(i), then $\gamma(i)$ is incremented downwards in small stages until one of the constraints (13.59) or (13.60) is impinged. With each trial value of $\gamma(i)$, δE_i is evaluated using equation (13.62) along with h(i-1) from (13.57) and hence $E^*_{i-1}\{h(i-1)\}$ may be obtained from a stored look-up table previously computed during the optimisation of the i-1 stage process. The minimum value of $\delta E_i + E^*_{i-1}$, and associated $\gamma(i)$ are selected, set equal to E^*_i and $\gamma(i)^*$ respectively and stored alongside h(i) whereupon h(i) is incremented and the procedure repeated until tables of $E^*_i\{h(i)\}$ and $\gamma(i)^*$ covering the entire field of interest have been computed. Attention is now transferred to the i+1 stage process and minimisation of E_{i+1} accomplished making use of the E^*_i table just obtained. At the conclusion of the exercise a sequence of energy minimising angles $\gamma^*(1), \gamma^*(2) \ldots \gamma^*(I)$ is obtained for any given h(I) from which the desired piecewise linear profile for the a.f.c is obtained using equation (13.57). Starting the entire procedure (i.e. with i set to unity) poses no difficulty in that all the entries in the E^*_o table are zero††

† Most physical modelling problems can usually be viewed as energy minimising problems to which the techniques of optimal control analysis are potentially applicable. For simple lumped parameter systems such an "energy approach" is generally more laborious than the conventional use of force, momentum, flow balance concepts however.

†† The foregoing discussion has presupposed free end conditions on h(o) and h(I). The computational sequence for i=1 and i=I would differ somewhat from the general procedure of Fig. 13.21 if the ends were fixed.

The computational sequences described above clearly need not be and in fact are not prohibitive in terms of their execution time and storage requirements if attention is restricted to, say, 20 trays with a height resolution of perhaps 0.5% of the peak undulation amplitude. The reason is that this problem involvesonly one state-and one control-variable so that the well known "curse of dimensionality" associated with higher order dynamic programming problems does not arise here. Stiffening of the deck-plate {i.e. inclusion of factor (b)} and incorporation of the relative - tilt constraint in the direction of face-advance {factors (d)} introduces some, but not excessive complication. The state order remains unaltered but we are now faced with two control sequences $\gamma(i)$ and $\alpha(i)$ $(i=1,2,...I)$ so that, associated with each E_i^* there will also exist a floating range of tilts

$$\alpha^*_1(i) < \alpha(i)^* < \alpha_2^*(i)$$

determined by incrementing $\alpha(i)$, for each chosen $\gamma(i)$, to find those values which cause either:

(i) contact with front and rear floors

or (ii) constraint $|\alpha(i) - \alpha(i-1)| \leqslant \Delta\alpha$ to be impinged.

An additional inner computational loop for varying $\alpha(i)$ is therefore involved and the constraint-testing procedures are now slightly more complicated.

If elasticity at the joints is permitted then the energy to be minimised becomes the total potential-plus-strain-energy so that if E_i now represents the <u>total</u> energy per pan

$$\delta E_1 = mg\{2h(i) + X_p\,\gamma(i)\} + k_d\{\delta\gamma(i)\}^2 + k_b\{\delta\alpha(i)\}^2 \qquad (13.64)$$

where the absolute elastic yields $\delta\gamma(i)$ and $\delta\alpha(i)$ are given by

$$\begin{aligned} \delta\gamma(i) &= |\gamma(i) - \gamma(i-1)| - \Delta\gamma \\ \delta\alpha(i) &= |\alpha(i) - \alpha(i-1)| - \Delta\alpha \end{aligned} \qquad (13.65)$$

and the stiffness coefficients k_a and k_b governed by

k_a = constant , $\delta\gamma(i) > 0$

= zero , $\delta\gamma(i) < 0$

k_b = constant , $\delta\alpha(i) > 0$

= zero , $\delta\alpha(i) < 0$

Joint elasticity therefore involves only slight complication of the cost function and minimal increase in program execution time.

The dynamic programming approach therefore holds great promise for a soundly-based rational solution to the problem of conveyor simulation. The a.f.c fitting routine is obviously run between simulations of the along-face dynamics described by equations (13.47) to (13.49) and (13.51) to (13.53).

13.3.4 Modelling for analytical predictions

Simulation of a complicated system is, of course, fraught with pitfalls and, even when properly running, can be laborious and time consuming if there exists no prior idea of the broad behavioural characteristics and the useful range of parameters to be explored. Analytic solutions, albeit of perhaps simplified systems, can be of enormous assistance in overcoming these difficulties, but, for many years, it was not appreciated how a multipass system might be rendered ammenable to solution by the control engineer's conventional techniques.

13.3.4.1 The use of long transport delays to model the interaction between passes.

A breakthrough leading to a more familiar form of model for multipass systems finally occurred when it was realised that the spatial coordinates n and ℓ are not independent variables in the sense that say, time and distance are independent in the more conventional distributed parameter systems (see chapter 2). In particular n and ℓ are not independent of one another since ℓ varies continuously but repeatedly in the range $0 < \ell < L$ integer n being incremented by a unit step with each resetting of ℓ. This means that any point specified by the two coordinates n, ℓ could alternatively be specified by the single coordinate v = total distance cut, (or passed) by the machine. In an undirectional cutting scheme such as

that illustrated in Fig. 13.22 in which the machine cuts only from left to right*, v is clearly given by

$$v = \ell + nL \tag{13.66}$$

The result of this realisation is that the dependent variables, say $y(n,\ell)$ or $h(n,\ell)$, at a point n,ℓ may be expressed alternatively as functions of v only, i.e. $y(v)$ and $h(v)$ respectively in this case. Extending the argument, $h(n-1,\ell)$ could for example be expressed in the new coordinate basis as $h(v-L)$. Process equations (13.47) to (13.49) may therefore be rewritten in the new basis as follows:

$$y(v) + z(v) = h(v+R) + W\alpha(v+R) + R\beta(v+R) + J(v) \tag{13.67}$$

where $$\alpha(v) = \{h(v) - h(v-L)\}/W \tag{13.68}$$

and $$\beta(v) = \{h(v) - h(v+F)\}/F \tag{13.69}$$

Additionally equation (13.50) describing the rubber conveyor could be re-expressed in the form

$$h(v + L) = y(v) + z(v)$$

so that $$h(v) = y(v - L) + z(v - L) \tag{13.70}$$

Likewise the control law (13.51) and equations (13.52) and (13.53) describing the sensor and actuator dynamics may also be expressed in terms of v rather than n and ℓ giving

$$J_d(v) = -k_h\, y(v) - k_g W\ \alpha(v+R) \tag{13.71}$$

$$d\, y_m(v)/dv = (1/X_1)\{y(v - X) - y_m(v)\} \tag{13.72}$$

and $$d\, J(v)/dv = (1/X_2)\{J_d(v) - J(v)\} \tag{13.73}$$

By taking Laplace Transform in s with respect to v of equations (13.67) to (13.73), a block diagram of transfer-functions involving lags X_1 and X_2 and transport delays X and L could clearly be obtained and manipulated to produce an open-loop system transfer-function which could be analysed for closed-loop system stability.

*Bidirectional schemes in which the machine cuts alternately in each direction are also ammenable to analysis[10] in terms of v but in this situation sampled-data system concepts must also be introduced.

As an example we shall ignore, for simplicity of presentation, the sensor and actuator dynamics so that (13.71) and (13.72) reduce to

$$y_m(v) = y(v - X) \tag{13.74}$$

and

$$J(v) = J_d(v) \tag{13.75}$$

so that the control law (13.71) becomes simply:

$$J(v) = -k_h\, y(v-X) - k_g\, W\, \alpha(v+R) \tag{13.76}$$

Again for simplicity we set $k_g = 1.0$ so that effect of the tilt, α, on the process behaviour is nullified and attention is restricted to the special case of the fixed-drum shearer so that offset R may be set to zero. Combining process equations (13.67) and (13.70) with control law (13.76) for this special case gives

$$y(v) + z(v) = y(v-L) + z(v-L) + J'(v) \tag{13.77}$$

where

$$J'(v) = -k_h\, y(v-X) \tag{13.78}$$

so that, in terms of Laplace transforms taken with respect to v, we obtain:

$$\tilde{y}(s) + \tilde{z}(s) = \{\tilde{y}(s) + \tilde{z}(s)\}\exp(-Ls) + \tilde{J}'(s) \tag{13.79}$$

where

$$\tilde{J}'(s) = -k_h \tilde{y}(s)\, \exp(-Xs) \tag{13.80}$$

yielding the block diagram given in Fig. 13.23. From the block diagram we see that the system may be regarded as a unity feedback system having the inverse open-loop transfer-function:

$$G^{-1}(s) = k_h^{-1}\, \exp(Xs)\{1 - \exp(-Ls)\} \tag{13.81}$$

Fig. 13.24 gives the form of the inverse Nyquist locus derived from equation (13.81) for the case of $X = L/12$, the closed-loop system being clearly unstable for all k_h since the inverse Nyquist stability criterion[10,14] requires that the net number of counterclockwise encirclements by $G^{-1}(s)$ of the point $-1 + j0$ in the plane of $G^{-1}(s)$, as s describes the usual clockwise semi circular excursion around the entire right-hand half s-plane, should equal the number of zeros of G(s) (=o in this case) within that half-plane.

13.3.4.2 Implicit approximations

The prediction of closed-loop instability by the delay model (13.81) accords completely with simulation experience and predictions are unaltered if the sensor and actuator dynamics are included in the analytical model, so confirming the simulation result given in Fig. 13.19. If X is set = L then from equation (13.81) we see that

$$G^{-1}(s) = k_h^{-1} \{\exp(Ls) - 1\} \qquad (13.82)$$

and from the resulting inverse Nyquist locus it is readily deduced that stability can now be obtained provided the positive gain k_h is restricted such that

$$k_h < 2.0 \qquad (13.83)$$

which again comfirms the results of simulation studies reported in Section 13.3.2. Indeed the modelling of the multipass process in terms of v and the consequent introduction of transport delays of duration L has proved to be a most reliable analytical means of predicting their behavioural characteristics generally. This is provided that

(a) the pass length L is always very much greater than the settling time of the transients occuring along the pass

and (b) attention is confined to transients induced at considerable distances from both ends of the pass.

These limitations are important so far as mathematical rigour is concerned and highlight the fact that the process equations (31.67) to (13.73) and all subsequent equations derived from them are in fact valid only for values of v in the ranges

$$nL + X < v \leqslant (n+1)L \quad , \quad n = 0,1,2.... \qquad (13.84)$$

since the sensor cannot commence measurement until $\ell > X$. For values of v within the ranges

$$nL \leqslant v \leqslant nL+X \quad , \quad n = 0,1,2.... \qquad (13.85)$$

the process is repeatedly reinitialised (i.e. reset) by boundary condition equations not considered hitherto but which might perhaps take the form

$$y(v) = h(v) = J(v) = y_m(v) = 0 \quad , \quad nL \leqslant v \leqslant nL + X \qquad (13.86)$$

if the machine were assumed to be properly "launched" at the start of each pass. This resetting action of course represents a series of discontinuities in the process occurring at intervals L which are completely disregarded in the continuous delay model presented in Section 13.3.4.1 and furthermore, this resetting would occur, albeit instantaneously, even if X = nL (n=0,1,2 etc) The delay model is therefore not suited to situations in which it allows transients to flow through from one pass to the next or in which the real life boundary conditions themselves induce transients. Owens[15] has presented an alternative view of the stability of multipass systems using the tehnqiues of functional analysis and has discussed the rigour of the delay model as a basis for stability prediction.

13.3.4.3 Approximate representation of conveyor "dynamics"

In Section 13.3.3 we considered carefully the modelling of the conveyor for computer simulation. This exercise yielded insight into the causes of conveyor stiffening but, without undertaking an exhaustive simulation programme, the model provides little insight into the likely effects on overall system behaviour. The model might reasonably be criticised on the grounds that it obscures the wood by the trees. Taking the broader view it is intuitively reasonable to expect that the introduction of some rigidity into the conveyor model might exercise a damping influence on the steering process because of the a.f.c's inability to follow precisely the shape of the cut floor beneath. Such an argument can however lead to a paradox because to work at all, the steering process relies on the flexibility of the a.f.c. Qualitative arguments cannot therefore settle the question as to whether or not the real-life steering system should be stable; or for what range of parameters stability might be expected. Approximate analytical models if logically constructed should, however, be capable of

indicating the degree of damping which might be anticipated from detailed simulations so justifying expensive simulation studies or showing them to be unworthwhile. It is the development of such analytical models (capable of integration into the delay model of the multipass process) which we now consider:

If the rubber conveyor equation (13.70) were modified to the slightly more general form

$$h(v) = k_a\{y(v - L) + z(v - L)\} \tag{13.87}$$

where k_a is an attenuating constant in the range

$$0 < k_a \leq 1.0 \tag{13.88}$$

then the transfer-function appearing in the interpass loop of Fig. 13.23 would be modified from $\exp(-Ls)$ to $k_a \exp(-Ls)$ and the inverse open-loop transfer function $G^{-1}(s)$ would become

$$G^{-1}(s) = k_h^{-1} \exp(Xs) \{1 - k_a \exp(-Ls)\} \tag{13.89}$$

so modifying the inverse Nyquist locus to the form shown in Fig. 13.25. This indicates that stability could now be achieved with positive controller gains k_h, provided

$$k_h < 1 - k_a \tag{13.90}$$

Attenuation of interpass coupling would therefore appear to be beneficial but the inclusion of merely the constant k_a takes now account of the fact that the a.f.c will respond differently to different frequencies and also to different amplitudes.

Fig. 13.26 illustrates the general shape which one edge of the a.f.c. would adopt (if unrestrained by the deck plate) in response to a sharp upward undulation in the cut floor

(a), beneath a pan joint and

(b), beneath a pan centre point

The illustration also shows curves closely fitting the true piecewise linear profiles and which could provide the basis for modelling the a.f.c.

by linear dynamics. Clearly a first-order linear system is capable of generating an impulse response resembling case (a) and perhaps an overdamped second-order system might generate that shown for case (b). Both cases exhibit fairly similar rates of decay however so that the two possible linear models would not differ drastically in their basic dynamics. The unique feature common to both impulse responses is however their symmetrical two-sided* nature. Such behaviour is not usually encountered in the study of physical dynamical systems but can occur in the field of off-line data processing.

Only bidirectional dynamical systems, i.e. those which process the input signal in both forward and backward time sequence, are capable of producing such two-sided responses. A system to produce the approximate impulse response shown in Fig. 13.26 (a), for instance, would operate on the input signal as follows

(i) the input data stream is stored

(ii) this data is now injected through a filter of transfer-function $0.5/(1 + X_c s)$, where X_c is the distance constant of decay, and the output stored

(iii) the original input data is fed from store in reverse-time sequence through an identical filter to that above and the output stored

(iv) the time sequence of the output data from step (iii) is reversed and the result stored

(v) the stored responses obtained from steps (ii) and (iv) are added and stored

(vi) the stored output from step (v) is fed out of the system after a total delay L from the commencement of the input signal.

*Obviously, if the floor impulse were off-centre the response would still be two-sided though no longer symmetrical. Floor disturbances will occur in practice with equal probability to left and right of centre however so justifying the use of a symmetrical impulse response approximation to the true response of the a.f.c.

Such a system cannot of course operate in real time unless it is associated with a long transport delay (the interpass delay L in this case). The frequency transfer function for the above process, provided

$$L >> X_c \tag{13.91}$$

is given by

$$H_c(j\omega) = \{0.5/(1+X_c j\omega) + 0.5/(1-X_c j\omega)\}\exp(-Lj\omega)$$

$$= \exp(-Lj\omega)/\{1 + (X_c\omega)^2\} \tag{13.92}$$

which would now replace the rubber conveyor transfer-function $\{= \exp(-Lj\omega)\}$ in the interpass loop of Fig. 13.23. Again for the validity of the model any disturbances considered must occur well away from the ends of the pass to prevent the a.f.c response from impinging on the process boundaries: a fuller mathematical discussion of this and related questions has been published by Edwards[11].

Whereas $G^{-1}(s)$ is unaffected[11] as Laplace variable s sweeps around the positive half s-plane at infinite radius, for $s = j\omega$ we now have that

$$G^{-1}(j\omega) = k_h^{-1} \exp(Xj\omega)\ \{1 - H_c(j\omega)\}$$

$$= k_h^{-1} \exp(Xj\omega)\ [1 - \exp(-Lj\omega)/\{1 + (X_c\omega)^2\}] \tag{13.93}$$

so that as ω increases towards the value $1/X_c$ the attenuation effect of the a.f.c rigidity becomes effective reducing the size of the lobes of the inverse Nyquist locus in the manner shown in Fig. 13.27 and opening up an area of stability for the siting of the critical point.

Stability may apparently be possible therefore if positive gain k_h is restricted such that

$$k_h < 1 - 1/\{1 + (\pi X_c/X)^2\} \tag{13.94}$$

so placing the -1 + jo point within the area of stability. The result therefore suggests that stability is potentially possible but there exists considerable uncertainty as the effective value for X_c. This value will of-course increase with signal amplitude indicating the possibility of limit cycling. All predictions made on the basis of this type of analytical

model must be regarded as tentative however because of the very considerable approximations made in its original formulation.

13.3.5 Other multipass processes

Other multipass processes are encountered in industry and generally involve the processing of some material or workpiece by repeated passes of the processing tool. In some cases the tool is stationary and the workpiece moves whilst in others the reverse situation applies. Examples include (i) the rolling - and (ii) the machining of metals. Example (ii) has much in common with (iii) the horizontal - (rather than vertical) steering of coal-face machines since high spots produced on pass n can cause the partial rejection of the cutting tool on pass n+1 because of the deeper penetration required, so possibly accentuating the original roughness. In these examples the interpass interaction comes about through the yield of the tool-positioning structure and should be small in well designed systems. The interaction between passes is therefore usually a comparatively weak secondary effect unlike the vertical steering system analysed previously in which such interaction is the primary effect. In applications (i) and (ii) however, and in the case of thin web machines - (iii) good surface finish can be a very important requirement so that the weak interpass effects must nevertheless be considered.

Another example of a related type is the automatic agricultural tractor which is steered to follow the previously ploughed furrow. The prediction of electrical load demand on power systems and the associated control of generation might also be viewed as multipass process because of the strong statistical correlations which exist between demand patterns (a) along the day in question and (b) across consecutive days.

The simulation of multimachine systems such as vehicle convoys, multi-stand rolling and paper mills etc. can also be conducted as a multipass process since a chain of identical transfer-function matrices (T.F.M's)

$\underline{G}(s)$ may be simulated by the repeated excitation of a single simulation cell of T.F.M $\underline{G}(s)$ from the stored (i.e. delayed) output from the previous simulation. The machines are thus simulated sequentially rather than simultaneously.

The concept may be extended as Edwards[16] has shown to the simulation of linear spatially distributed systems approximated in the manner of Chapter 2 by a chain of similar discrete simulation cells.

The stability and dynamic response of all such systems may therefore be investigated using delay models of the type developed in the previous Section. Although presented here in a specifically mining context it is hoped that through this discussion the reader will appreciate the relevance of the suggested modelling approach to a much wider class of problems. The analogy with two dimensional data processing systems has also been mentioned in section 13.3.4.3 and the wealth of theoretical analysis[17][18] published in this area may also be usefully brought to bear on those multi-pass processes of a more physical type.

13.4 Clearance Systems

We now turn attention outbye from the winning faces towards the mine shaft or drift up which the coal or mineral is conveyed to the surface for preparation for market. The system for transporting the material between these two points is known as the clearance system and constitutes a network of conveyors and fixed intermediate bunkers for smoothing out bottlenecks. The conveyors may be continuous, i.e. belt conveyors or discrete, e.g. shuttle cars or trains of tubs or mine-cars hauled by winches or locomotives. Discrete types of conveyor or variable-speed belts may also serve temporarily as bunkers and some bunkers can, as we shall see in Section 13.4.2. also resemble conveyors to some extent rather than being simple hoppers. The distinction between the purely storage function and the purely transportation function can therefore become somewhat blurred in practice.

The individual entities of the clearance system can pose interesting local control problems demanding very detailed modelling of the sub process itself and an example of this is considered in Section 13.4.2. A somewhat less detailed but wider ranging model of the clearance network itself, or a substantial portion of it, is also necessary as an aid to the synthesis of central (computer) control systems for the supervision of the overall production from the mine. The question of decomposition of a complex network into handlable units naturally arises and the provision of a large bunker can often serve to define the boundary between such units. Underground bunkers are however extremely expensive to install because of the cost of the large excavations needed for their accommodation and it is therefore worthwhile to consider whether or not sophisticated flow-control of a more comprehensive sort might not obviate the need for an enormous bunker. By implication therefore the size of the bunker may be left unspecified at the control-design stage and the bunker cost be included as one term of an overall cost function to be minimised. Having determined the integrated optimal control strategy for the entire network the necessary optimal bunker sizes can then be determined by simulation. (The alternative approach more commonly practiced is to simulate, on a cut-and-try basis, arbitrarily sized bunkers and control systems of a simple localised type to determine the best of the guessed combinations none of which are likely to provide a globally optimal performance).

13.4.1 Modelling clearance systems for optimal control synthesis

Fig. 13.28 illustrates an elementary clearance system comprising two winning faces (a) and (b) supplying mineral to a common drift via trunk conveyors involving transport delays T_a and T_b respectively. We shall assume that a constant volumetric rate $f_c(t)$ is demanded by the drift conveyor, any excess delivery from the trunk conveyors being accommodated by a pit bottom bunker as shown and any deficiency made up from the bunker. If $f_a(t)$ and $f_b(t)$ denote the instantaneous

production rates from the winning machines (a) and (b) respectively then if F(t) is the volumetric contents of the bunker it is obvious that

$$dF(t)/dt = f_a(t - T_a) + f_b(t - T_b) - f_c(t) \qquad (13.95)$$

the variables being subject to the overriding constraints that

$$F(t) \ , \ f_a(t) \ , \ f_b(t) \ , \ f_c(t) > 0 \qquad (13.96)$$

Now the machine speeds and hence $f_a(t)$ and $f_b(t)$ are controllable for much of the time but production is halted cyclically during face-end manoeuvres and also randomly particularly during periods of unfavourable geological conditions at the face when machine progress may be temporarily halted by roof fall or damage to equipment. The face production rates may therefore be described by the equations

$$\begin{aligned} f_a(t) &= d_a(\ell_a,t)\ u_a(t) \\ f_b(t) &= d_b(\ell_b,t)\ u_b(t) \end{aligned} \qquad (13.97)$$

where $u_a(t)$ and $u_b(t)$ are the demanded production rates adjusted by manipulation, when possible, of the machine haulage speeds $v_a(t)$ and $v_b(t)$, (no distinction between the speeds of the two ends of the haulage transmission is necessary here because the haulage system dynamics discussed in Section 13.2 are far faster than those of the clearance system). The variables $d_a(\ell_a,t)$ and $d_b(\ell_b,t)$ switch between the values of unity and zero, partly randomly in time for reasons mentioned above and partly cyclically in distance ℓ_a and ℓ_b at face-length intervals L_a and L_b. The along-face distances are of course governed by the differential equations

$$\begin{aligned} d\ell_a(t)/dt &= v_a(t) = f_a(t)/W_a \\ d\ell_b(t)/dt &= v_b(t) = f_b(t)/W_b \end{aligned} \qquad (13.98)$$

(where W_a and W_b denote the web thicknesses) and the constraints

$$\begin{aligned} 0 < \ell_a < L_a \\ 0 < \ell_b < L_b \end{aligned} \qquad (13.99)$$

The statistical properties of face-stoppages have been exhaustively studied in the U.K. and European coal mining industries and incorporated

into a number of computer simulation packages[19,20,21] for the study of clearance system behaviour. For control system synthesis, however, the random stoppage signals (d_a and d_b in this case) have to date only been modelled[21,22] by white noise fed into low-order colouring filters whose time constants match the mean time-between-stoppages and mean stoppage-duration. The cyclic component could no doubt be incorporated fairly readily by employing a second-order oscillatory model of appropriate natural frequency though the distance-base might pose problems.

The prime costs to be balanced in the optimisation of a coal clearance system are the costs of production which are basically flow-rate dependent and cost of bunkerage which are dependent on stickpile sizes. If F_c denotes bunker capacity therefore the performance index to be minimised might reasonably take form, in our example,

$$C(f_a,f_b,T_f) = \int_o^{T_f} \left[\lambda_1\{f_a^i(t) + f_b^i(t)\} + \lambda_2 F_c^j\right] dt$$

$$= \lambda_2 \int_o^{T_f} \left[F_c^j + \lambda\{f_a^i(t) + f_b^i(t)\}\right] dt \qquad (13.100)$$

where

$$\lambda = \lambda_1/\lambda_2 \ , \qquad (13.101)$$

λ_1 being the total annual cost of the winning and conveying machinery (p.u. flow rate^i) including electricity costs, interest, depreciation and maintenance costs etc. and λ_2, the total annual cost of bunkerage (p.u. stored-volume^j). The parameters λ_1 and λ_2 may be fitted after a careful study of available cost data. T_f is the period over which the process is to be optimised this being at least the duration of a production shift and longer in the case of continuous (3-shift) production. In the interests of ease of solution of the optimal control problem, i.e. that of minimising C by choice of input functions $u_a(t)$ and $u_b(t)$ it is tempting to choose indices i = j = 2 but in practice i should probably be of greater magnitude

and j nearer unity since bunker costs are likely to depend more or less linearly on F_c whereas the penalty for overloading electrical machines, in terms of reduced life expectancy and the consequential losses of production through insulation failure, tends to occur more abruptly with increasing load than the quadratic index would suggest.

The block diagram for the system of Fig. 13.28 is shown in Fig. 13.29 but for optimal control calculations it is preferable to relegate the transport delays to the output-end of the diagram as shown in Fig. 13.30. Provided $T_f >> T_a$ or T_b as in this application, this step results ultimately in a control law demanding feedback from only the ends of the conveyor delays and not from intermediate points along the conveyors - as Noton[13] has demonstrated and we shall see shortly in a simple example. The optimisation of large networks is most conveniently accomplished by the use of discrete dynamic programming techniques[13,21,22] necessitating the modelling of the conveyors T_a and T_b by n and m discrete slices respectively as indicated in Fig. 13.30 where

$$n = T_a/\Delta T \text{ and } m = T_b/\Delta T \tag{13.102}$$

ΔT being the time step for the computations and selected to be considerably smaller than T_a or T_b. (The model now resembles a continuous train of fixed-speed mine cars with variable filling). A state transition matrix model of the form

$$\underline{x}\{(i+1)\Delta T\} = \underline{\Phi}(\Delta T)\ \underline{x}(i\Delta T) + \underline{\Delta}(\Delta T)\ \underline{u}(i\Delta T) \tag{13.103}$$

where $\underline{x}$ is the state vector and $\underline{u}$ the input vector ($= [u_a, u_b]^T$) is now formed from the n equations of delay T_a, viz

$$\begin{aligned} x_{a,1}\{(i+1)\Delta T\} &= x_a(i\Delta T) \\ x_{a,j}\{(i+1)\Delta T\} &= x_{a,j-1}(i\Delta T)\ ,\ 1 < j \leqslant n \end{aligned} \tag{13.104}$$

and m similar equations in $x_{b,j}$ for delay T_b, together with the 2p state equations describing the dynamics of the pth order colouring filters describing d_a and d_b and the state equations

$$x_a\{(i+1)\Delta T\} = x_a(i\Delta T) + \Delta T\, f_a(i\Delta T)$$
$$x_b\{(i+1)\Delta T\} = x_b(i\Delta T) + \Delta T\, f_b(i\Delta T) \qquad (13.105)$$

$$x_c\{(i+1)\Delta T\} = x_c(i\Delta T) + \Delta T\, f_c(i\Delta T) \qquad (13.106)$$

$$f_c\{(i+1)\Delta T\} = f_c(i\Delta T) \qquad (13.107)$$

d_a and d_b are now approximated to additive rather than modulating disturbances so that

$$f_a(t) \simeq d_a(t) + u_a(t)$$
$$\text{and } f_b(t) \simeq d_b(t) + u_b(t) \qquad (13.108)$$

The state vector $\underline{x}$ is therefore of order n+m+2p+4 and the process model is clearly obtainable in the linear form of state-transition equation (13.103).

As regards the cost model (13.100), if i and j = 2.0 we have the convenient integral quadratic function of state and input variables, provided bunker capacity F_c can be linearly related to F(t). Ideally of course F_c should represent the upper limit of F(t) but provided occasional spillage and conveyor shut-down can be tolerated then F_c might be equated to the root-mean-square value of F(t) so allowing a reasonable margin for filling above the mean level $\overline{F}$ and only a low probability of emptying the bunker. We therefore define F_c as follows

$$F_c^2 = \underset{T_f \to \infty}{\text{Lim}} \int_o^{T_f} \frac{F^2(t)}{T_f}\, dt \qquad (13.109)$$

so permitting the replacement of F_c^2 by $F^2(t)$ in (13.100). In simulating the optimised system it is found however that $\overline{F}$ settles at a negative value so contravening constraint (13.96). The problem is readily overcome by noting that

$$\underset{T_f \to \infty}{\text{Lim}} \int_o^{T_f} \frac{F^2(t)}{T_f}\, dt = \underset{T_f \to \infty}{\text{Lim}} \int_o^{T_f} \frac{\{2\overline{F} - F(t)\}^2}{T_f}\, dt = \overline{F}^2 + \sigma_F^2 \qquad (13.110)$$

{where σ_F denotes the standard deviation of $\overline{F} - F(t)$}

and hence substituting $\{2\overline{F} - F(t)\}^2$ for F_c^2 in the performance index. The fact that $\overline{F}$ is the unknown a priori is unimportant, its value being deter-

mined in the course of simulation of the optimal control law. It is merely necessary to increase ref. signal $2\overline{F}$ progressively until the probability of emptying the bunker is reduced to an acceptably low level. The performance index in summation form therefore becomes, from (13.100) (13.95) (13.104) (13.105)(13.106) and (13.110)

$$C = \lambda_2 \sum_{i=o}^{T_f/\Delta T} \left[\{ 2\overline{F} - x_{a,n}(i\Delta T) - x_{b,m}(i\Delta T) + x_c(i\Delta T) \}^2 \right.$$

$$\left. + \lambda \{ f_a^2 (i\Delta T) + f_b^2 (i\Delta T) \} \right] \Delta T \qquad (13.111)$$

The modelling of clearance system in the manner indicated and the application of dynamic programming (a very efficient version[13] of which has been specially tailored to the optimisation of linear processes subject to quadratic costs) has been found to yield very successful control strategies ideally suited to central computer control and which perform well dynamically and economically not only on the linearised plant models but also on the original nonlinear system. Furthermore the resulting control rules are reducable to a very straightforward physical interpretation. This is now demonstrated with the aid of a simple clearance system example involving only one winning machine.

13.4.1.1 A simple example

Channel (b) of the winning and clearance system of Fig. 13.28 is here removed leaving only channel (a). In the foregoing equations therefore terms involving suffix (b) are set to zero and suffix (a) being now unnecessary is dropped from the notation. This simple system is amenable to solution by pencil and paper methods using Pontryagin's maximum principle, as will be briefly outlined, and there is therefore no need in this particular case to discretise the process equation and cost integral. Our problem is therefore that of minimising, by choice of u(t) the cost function

$$C(t) = \lambda_2 \int_0^\infty \left[\{2\bar{F} - x(t-T) + x_c(t)\}^2 + \lambda f^2(t)\right]dt$$

where $f(t) = u(t) + d(t)$

and the state equations are

$$dx(t)/dt = u(t) + d(t) \qquad (13.112)$$

and $$dx_c(t)/dt = f_c = \text{constant} \qquad (13.113)$$

Now considering the cost of bunkerage we note that

$$\int_0^\infty \{2\bar{F} - x(t-T) + x_c(t)\}^2\, dt = \int_{-T}^\infty \{2\bar{F} - x(t) + x_c(t) + f_c T\}\, dt$$

$$+ \int_0^\infty \{2\bar{F} - x(t) + x_c(t) + f_c T\}\, dt$$

and since the first integral on the right-hand-side (above) cannot be controlled by $u(t)$, $t > o$ we confine attention to minimising

$$C = \lambda_2 \int_0^\infty \left[\{2\bar{F} - x(t) + x_c(t) + f_c T\}^2 + \lambda\{u(t)+d(t)\}^2\right]dt$$

By the maximum principle of Pontryagin this implies maximising the Hamiltonian:

$$H = p(t)\{u(t)+d(t)\} - \left[\{2\bar{F} - x(t)+x_c(t)+f_c T\}^2 + \lambda\{u(t)+d(t)\}^2\right]$$

where costate $p(t)$ is governed by

$$dp(t)/dt = -\partial H/\partial x = 2\{x(t)-x_c(t)-f_c T - 2\bar{F}\} \qquad (13.114)$$

For maximum H we set $\partial H/\partial u = o$ giving

$$2\lambda \{u(t) + d(t)\} = p(t) \qquad (13.115)$$

For the optimim control profile $u(t)$ we must therefore solve (13.112) to (13.114) simultaneously in reverse time $\tau(=T_f - t)$. As $\tau \to \infty$ we find that

$$u(\tau) + d - f_c \to -(1/\sqrt{\lambda})\{x(\tau) - x_c(\tau) - 2\bar{F} - f_c T\}$$

$$\to \{x(o) - x_c(o) + \sqrt{\lambda}\, f_c - 2\bar{F} - f_c T\} \exp(\sqrt{\lambda}\tau)/2 \qquad (13.116)$$

and since $F(t) = x(t-T) - x_c(t)$, the control law (13.116) may be expressed

$$u(t) = -d(t) + f_c(t) - (1/\sqrt{\lambda})\{x(t) - x(t-T) + F(t)\}$$

$$+(1/\sqrt{\lambda})\{2\bar{F} + f_c T\} \qquad (13.117)$$

The mean level $\bar{F}$ therefore appears as a reference signal as expected to be set in simulation. The term $\{x(t) - x(t-T) + F(t)\}$ is very interesting being the <u>total</u> mineral stored instantaneously in the bunker and on

the conveying system. F(t) may be measured directly and the conveyor storage term computed from a single belt weigher together with a digital delay and integration routine. The control law is therefore highly practical, calling for feedback of "total system storage". Analysis of the control law by means of inverse Nyquist techniques[23] reveals it to be non-resonant, yet not overdamped, for a very wide range of cost ratios, λ.

This simplified example has not brought out the need for machine load-control with which we were preoccupied in Section 13.2 of this chapter. This is partly because of our neglect of the dependence of cost weighting, λ, on the variable mineral hardness. As Edwards has shown[22] however, load-control does appear if the thermal time-constants of the production machines are modelled, and the cost of overtemperature penalised rather than merely the instantaneous production rates. The resulting control of the process is a good compromise between the conflicting requirements of the clearance system and the production machines, and takes advantage of the inherent overload-capacity of electrical machines to sustain mine output during periods of interruption of supply from other faces.

13.4.2 The modelling of a horizontal bunker conveyor

Global network models of the type described in the previous Section of this chapter are simplistic in that they take for granted the operation of local control loops for the manipulation of flow-rates from feeders, levels in bunkers, cutting-machine speeds etc. These local loops can, however, involve unit sub-processes, the dynamic behaviour of which can be highly complex. This was evident in our study of coal-cutting dynamics earlier in the chapter. In the clearance system too individual equipments can pose local modelling and control problems which are far from trivial and which must be solved for the mine to operate in any fashion, optimally, or otherwise. The horizontal bunker conveyor is one such example which,

as will be seen, operates in a manner which is far more complex than might be envisaged from a higher level in the control hierarchy where the bunker is viewed conceptually as a simple hopper.

Fig. 13.31 illustrates such a bunker diagramatically and indicates the main variables required for its mathematical description. Mineral enters the bunker randomly at a volumetric flow-rate $f_i(t)$ directly into the exit-well which supplies the vibrating feeder from which mineral is discharged to the output conveyor as shown. It will be assumed in this analysis that the output rate $f_o(t)$ can be independently manipulated although in practice this implies the existance of a tightly-tuned control loop around the vibro-feeder and incorporating a weigher on the output belt situated some distance downstream. This is generally essential to compensate for the effect of varying well-height, $h_e(t)$, and mineral quality on $f_o(t)$. Even in this minor loop however, considerable modelling and control problems are posed.[24]

Any excess of inflow may be drawn into the bunker by setting velocity $v(t)$ to a negative value whilst a reduced inflow may be compensated by means of mineral tipped back into the exit-well from the bunker, i.e. by making $v(t)$ positive. Delivery to and from the bunker tends to occur in discrete slices of horizontal thickness Δx (typically 0.6 m but depending on mean particle-size and moisture-content). In practice the slices tend to be separated by inclined shear-planes but we shall assume these to be vertical for simplicity of analysis. The heights of the individual slices are variable in an uncontrolled situation and, as indicated in Fig. 13.31 are denoted by $h_b(i)$, where integer i takes the range of values:

$$i = 1,2,3...n \tag{13.118}$$

where n is the number of slices in the bunker at time t, being constrained such that

$$1 < n < N \tag{13.119}$$

where N is the total number of slices that the bunker can accommodate.

In modelling it is therefore assumed that, if W is the bunker width, each time, t_n, the bunker moves forward by a distance Δx a volume of mineral $W\Delta x\, h_b(n)$ is tipped into the exit well and the number n is decremented by 1.0. Each time the bunker travels backwards by distance Δx however a slice of height $h_e(t_n-)$ is transferred to the bunker from the exit well and the well contents falls abruptly in volume by an amount $W\,\Delta x\, h_e(t_n-)$, where t_n- denotes the time marginally before the material transfer occurs. The derivative of $h_e(t)$ therefore changes impulsively with each material-transfer so that, if A is the cross sectional area of the well, the behaviour of $h_e(t)$ may be described by the differential equations

$$A\, dh_e(t)/dt = f_i(t) - f_o(t) + W\Delta x h_b(n)\, \delta(t-t_n)\ ,\ v(t_n-) > 0 \qquad (13.120)$$

or

$$A\, dh_e(t)/dt = f_i(t) - f_o(t) - W\Delta x h_e(t_n-)\delta(t-t_n)\ ,\ v(t_n-) < 0 \qquad (13.121)$$

where

$$h_b(n) = h_e(t_n-)\quad ,\quad v(t_n-) \lessgtr 0 \qquad (13.122)$$

and the transfer-time t_n is given by

$$\int_o^{t_n} v(t)dt = n\Delta x \qquad (13.123)$$

$\delta(t-t_n)$ dentoes a unit impulse function occurring at $t = t_n$.

Real time simulation of the system is highly desirable for operator training and for the investigation of automatic control schemes. Equation (13.120), (13.21) and (13.123) are readily simulated on an analogue computer equipped with elementary logic to detect incremental bunker movements exceeding Δx, the sign of $v(t_n-)$ and to switch in the impulse function at the appropriate instants t_n. Simple analogue control systems based on measurements of $h_e(t)$ are likewise ammenable to analogue simulation. Since N is a large integer (100 to 200 for example) the storage of the bunker-height profile $h_b(i)$, $(i = 1,2...n)$, however, requires the use of a digital computer interfaced to the analogue machine via appropriate

converters. Elements are added to the array $h_b(i)$ whenever $v(t_n-) < 0$ and withdrawn whenever $v(t_n-) > 0$ in accordance with equations (13.120), (13.121) and (13.122).

Fig. 13.31 illustrates the behaviour of the bunker controlled according to control law (13.124), the purpose of which is to attempt to maintain the bunker level as close as possible to reference h_r. The control law is expressed thus

$$v(t) = k_p\{h_r - h_e(t)\} + k_i \int_o^t \{h_r - h_e(t)\}dt \qquad (13.124)$$

where k_p and k_i are the proportional and integral gains of the controller and Fig. 13.32 shows the system response when disturbed by step-changes in $f_i(t)$ as shown. The system parameters are W = 2m, A = $4m^2$ Δx = 0.4m, h_r = 1.5m. The reduction in $f_i(t)$ from 600 to 540 tonne/hr is clearly compensated, after a transient dip in h_e and h_b, by a reduction in absolute velocity: as evidenced by the reduced frequency at which slices enter the bunker. The fall of $f_i(t)$ to 420 tonne/hr, i.e. below the constant output rate of 480 tonne/hr, is also clearly compensated after a considerable transient by a reversal of the bunker role from filling to emptying. Interesting features of the process dynamics are :

(a), that transients created in the $h_b(i)$ profile whilst the bunker is filling, will ultimately return to disturb the control system when the bunker is emptying, and

(b) that whereas the uncontrolled process is of a fundamentally self-regulating nature during the filling operation {the heights $h_b(i)$ and $h_e(t)$ settling to some constant value for constant v(t), $f_i(t)$ and $f_o(t)$}, its dynamics change to an integrating type during emptying. The controller parameters for satisfactory filling are therefore not necessarily applicable whilst emptying and indeed stability in both modes is difficult to achieve with constant controller parameters.

Similar modelling techniques could readily be applied to other mineral-handling processes which share the same principle of operation such as the filling and emptying of trains of mine cars for instance. In some instances the last car filled might be the first to be emptied, so involving the "record-and-reverse" procedure used to simulate the conveyor bunker. In other cases, when filling and emptying take place in the same sequence, the storage process will resemble a transport delay but physically discretised in a manner resembling our earlier mathematical segmentation of the continuous conveyor belt.

13.5 Discussion

The chapter has illustrated the novelty of the models of mining processes occuring throught the mine from the winning face to the pit-bottom. Despite this apparently special nature of mining processes, important links with processes outside the mining field have, however, been identified. We have, for example, noted similarities in the dynamics of mineral cutting with those occurring in the machining of metals. The multipass nature of longwall coal mining is a characteristic which has been shown to be shared by various repetitive processes, industrial and otherwise. The techniques for developing mining process models, whether for direct simulation, analytical solution or controller synthesis, can therefore be usefully applied outside the mining field and should therefore be of general interest.

Special characteristics which have appeared throughout the chapter have included long transport delays associated with a variety of phenomena including regenerative cutting dynamics, multipass operations and conveying. Their incorporation into models for simulation and for solution by frequency-response analysis and optimal control design techniques has been demonstrated, producing worthwhile control results and a good degree of insight into why the systems behave as they do. Also encountered has been the "record and reverse" process - associated with bidirectional coal-face operation, the

representation of face-conveyor dynamics and in modelling bunker and train dynamics. Its incorporation into simulation has been demonstrated and it can generally be incorporated into analytical studies although this has here been restricted to face-conveyor studies.

13.6 References

(1) Welbourne, D.B. and Smith J.D., 'Machine tool dynamics, Cambridge University Press, 1970.

(2) Merritt, H.E. and Hohn, R.E., 'Chatter, another control problem', Control Engineering, December 1967, pp. 61-64.

(3) O'Dogherty, M.J. and Burney, A.C. Colliery Engineering,Feb. 1963, 40, pp. 51-54 and March 1963, pp. 111-114.

(4) Evans, I. and Pomeroy, C.D., 'Strength, fracture and workability of coal', Pergamon Press, Oxford, 1966.

(5) Pomeroy, C.D. 'Breakage of coal by wedge action - factors affecting tool design', Colliery Guardian, July 1964, 209, pp. 115-121.

(6) Edwards, J.B. 'Modelling the dynamics of coal and mineral cutting', Proc. I. Mech. E., 1978, Vol. 192, No. 30, pp. 359-370.

(7) Dowell, J. and Edwards, J.B., 'Development of the Bretby external haulage', Mining Electrical and Mechanical Engineer, Jan. 1968, 49, No. 567, pp. 3-17.

(8) Cooper, L.R. 'Gamma-ray backscatter gaugues for measuring coal thickness on mechanical coal faces, Proc. of I.E.E. International Conference on Industrial Measurement and Control by Radiation Techniques, Guildford, 1972, I.E.E. Conf. Pub. No. 84, pp. 89-93.

(9) Edwards, J.B. and Addison G.J. 'The nucleonic coal sensor as an element of a control system for automatic steering of a coal cutter', ibid, pp. 20-29.

(10) Edwards, J.B. 'Stability problems in the control of multipass processes', Proc. I.E.E., 1974, Vol. 121, No. 11, pp. 1425-1432.

11) Edwards, J.B. and Greenberg, J.M. 'Longitudinal interactions in multipass processes', Proc. IEE, 1977, Vol. 124, No. 4, pp. 385-392.

12) Bogdadi, W.A. and Edwards, J.B. 'The automatic vertical steering of a longwall coal-cutting machine - an experimental investigation', Proc. I.Mech.E., 1975, Vol. 189, 32/75, pp. 187-195.

13) Noton, A.R.M. 'Variational methods in control engineering', Pergamon Press, London, 122.pp.

14) Shinners, S.M. 'Control system design', Wiley, New York, 1964, 523 pp.

15) Owens, D.H. 'Stability of linear multipass processes', Proc. I.E.E., 1977, Vol. 124, No. 11, pp. 1079-1082.

16) Edwards, J.B. 'Wider application of multipass systems theory', Part 1, Multimachine and multicell systems, and Part 2: Controlled distributed processes', Proc. I.E.E., 1978, Vol. 125, No. 5, pp. 447-452 and pp. 453-459.

17) Jury, E.I. 'Stability of multi-dimensional scalar and matrix polynomials', Proc. I.E.E.E., 1978, Vol. 66, NO. 9, pp. 1018-1047.

18) Boland, F.M. and Owens, D.H., 'Linear multipass processes: a two-dimensional interpretation', Proc. I.E.E. - to be published.

19) Mitchell G.H. and Lee J.R. 'Digital Simulation in Operational Research: Simulation applied to underground transport problems in collieries of the National Coal Board', Hollingdale S.H. (ed), English Universities Press, London.

20) Ranyard, J.C., 'Locomotive coal transport study', Chap. 4, Ph.D. Thesis, 1972, University of Lancaster, pp. 45-52.

21) Fawcett, W., 'Simulation and control of coal production and transport', Ph.D. Thesis, University of Sheffield, 1975.

22) Edwards, J.B. and Marshall, S.A. 'Integrated plant and control system design for the operation of a mine at minimum cost', Proc. of I.F.A.C., International Symposium on Automatic control in mining mineral and metal processing, Sydney, Australia, Aug. 1973.

23) Edwards, J.B. 'Optimal control strategies for systems of multiple bunkers, conveyors and supply points', Proc. of I.E.E. Conference on Measurement and control in the handling and processing of materials, London, April, 1978, pp. 153-160.

24) Dowell, J. and Park, A.H.D. 'The design and performance of control systems for horizontal bunkers and bunker conveyors', ibid, pp. 113-120.

13.7 Acknowledgements

The modelling of a.f.c. behaviour by dynamic programming described in Section 13.3.3 was first undertaken by the author as part of a National Coal Board (N.C.B) research contract. The N.C.B's permission to publish the material of Section 13.3.3 in the present text is gratefully acknowledged. It is also acknowledged that substantial portions of the remainder of the chapter were originally reported by the author in references (6) to (7), (9) to (12), and (22) to (23) but with the emphasis there on stability and control rather than on process modelling as such.

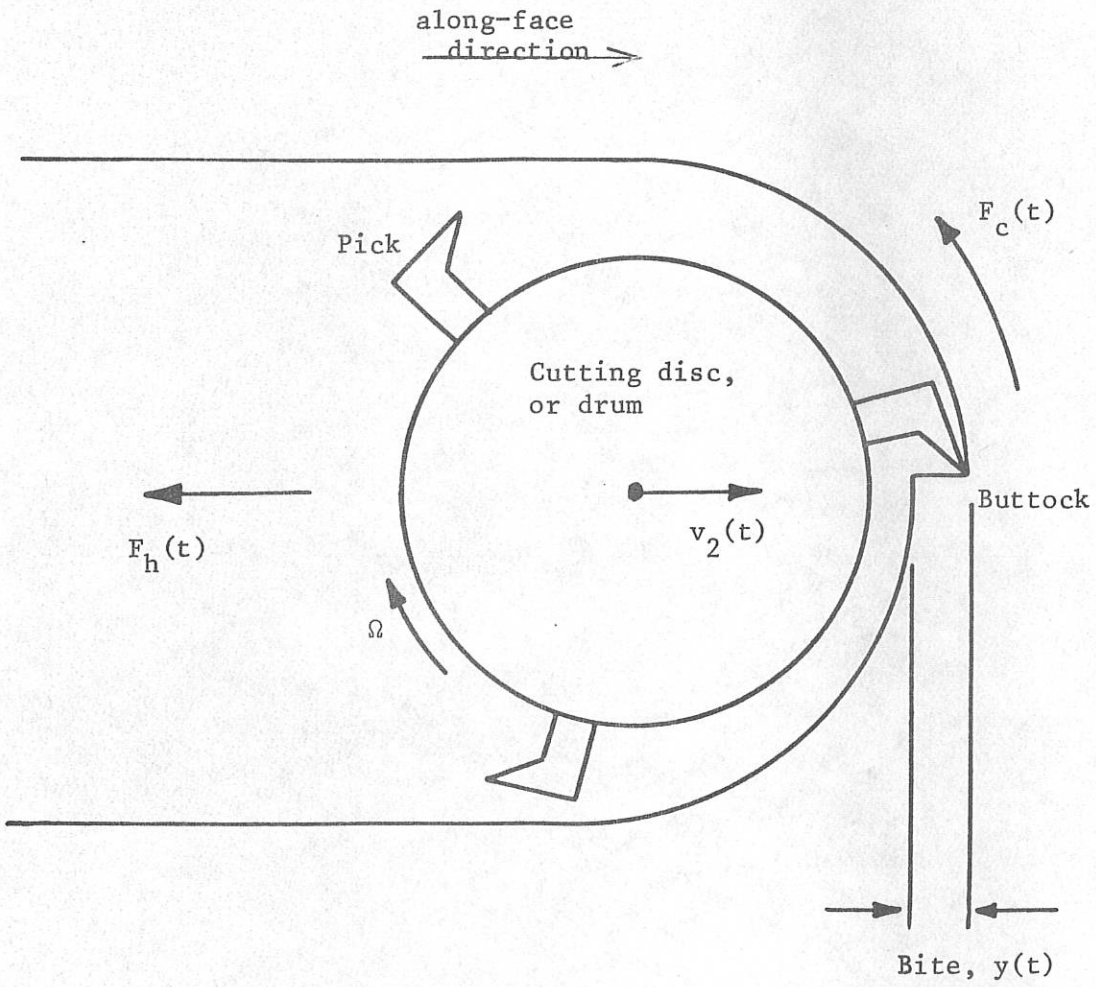

Fig. 13.1 Showing cutting action of a miller or shearer machine.

(a) Trepanner head viewed in direction of machine travel.

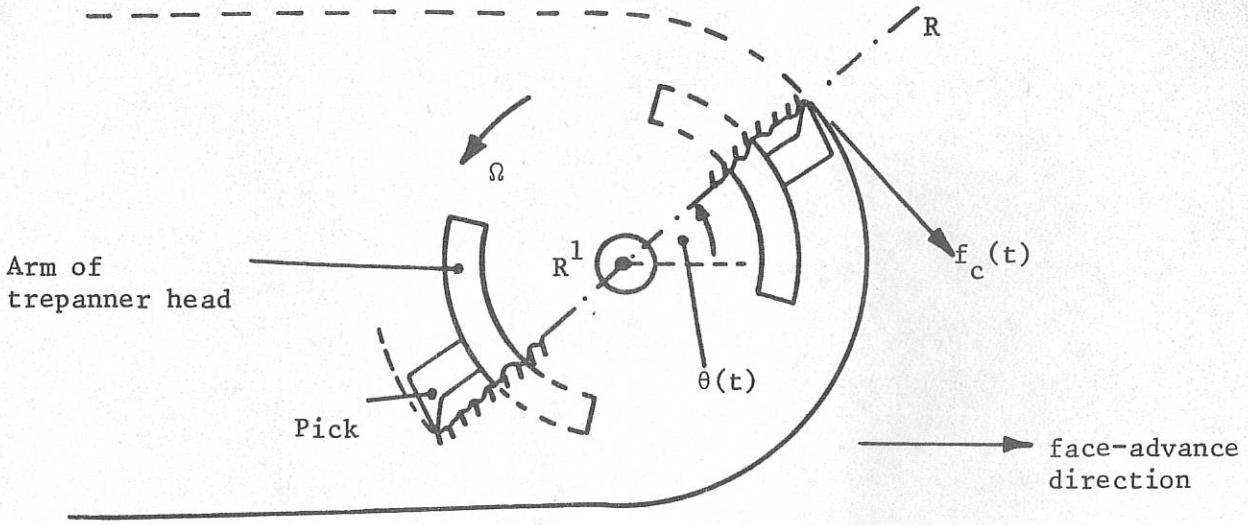

(b) Trepanner head viewed in direction R R^1.

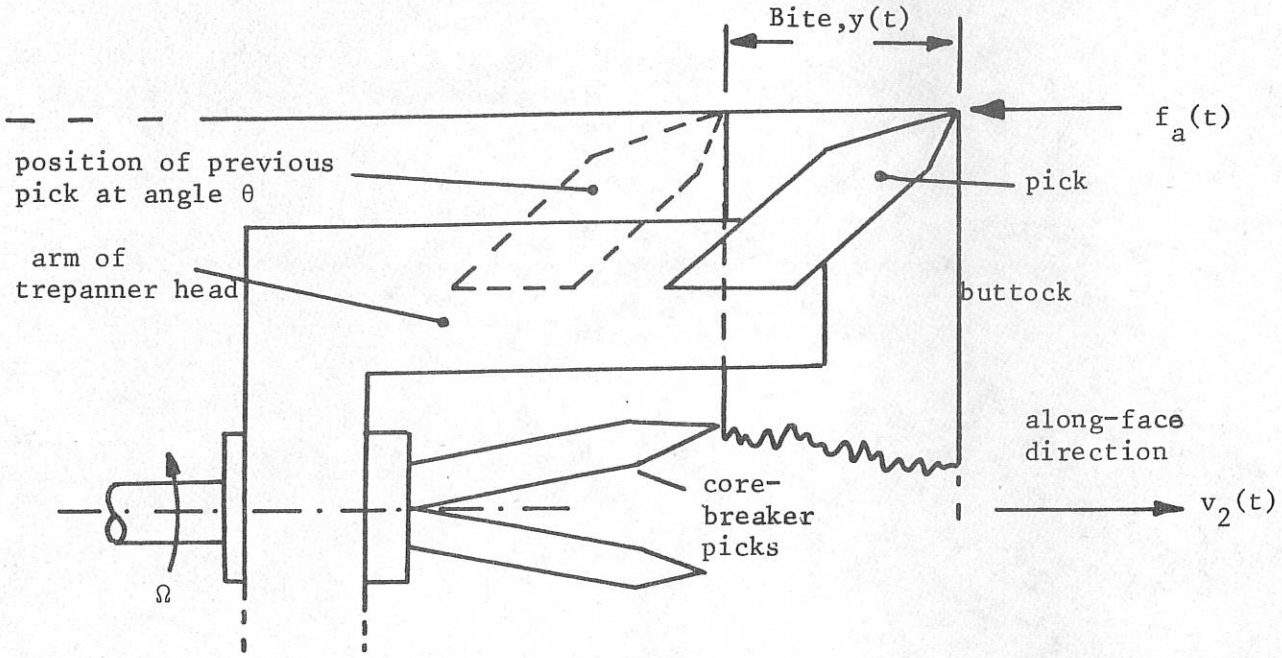

(c) Relative poisitions of trepanner head on consecutive cuts.

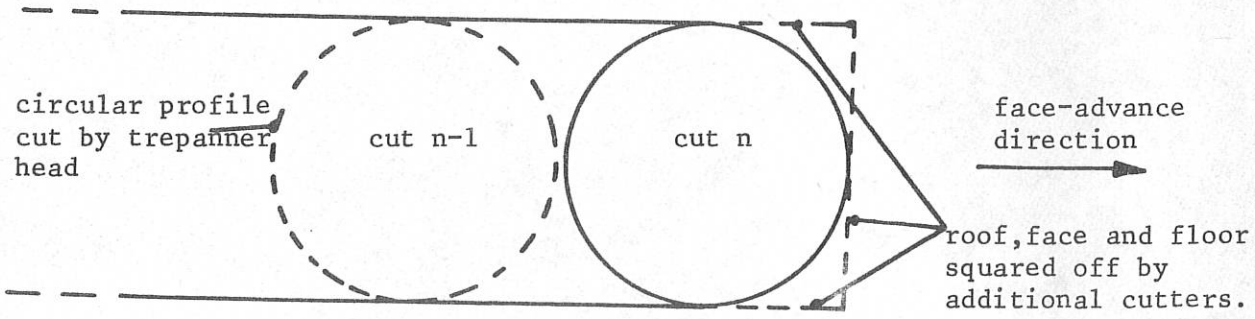

Fig. 13.2 Trepanner cutting action

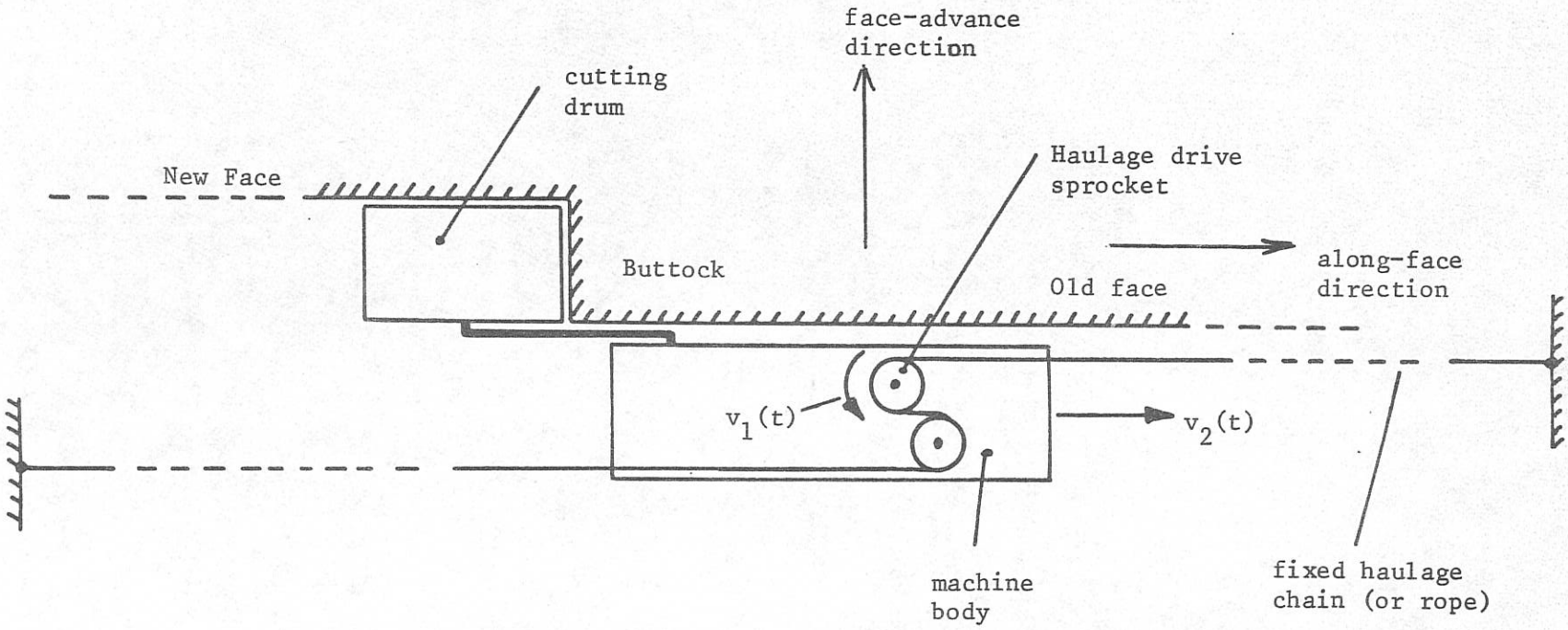

Fig. 13.3 Plan view of shearer machine showing inbuilt haulage system

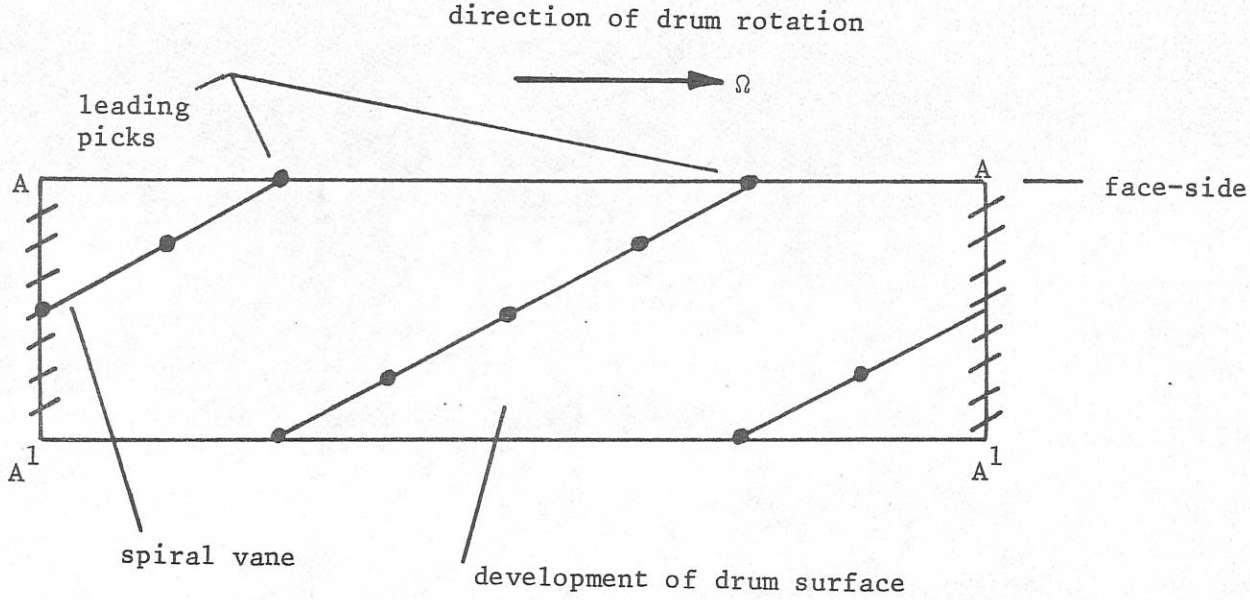

Fig. 13.4 Spiral pick-lacing pattern for a shearer drum

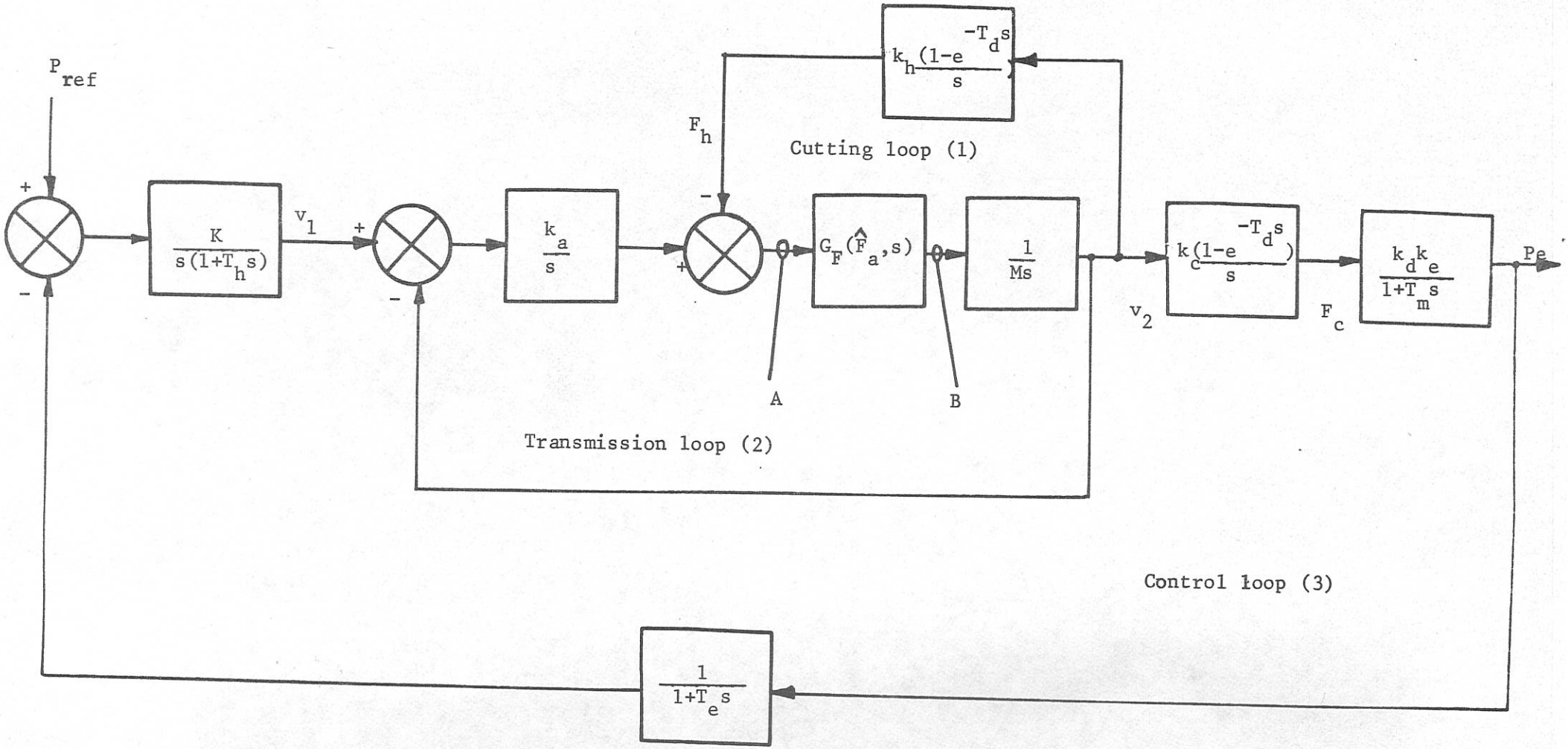

Fig. 13.5 Block diagram of automatically controlled cutting and haulage system

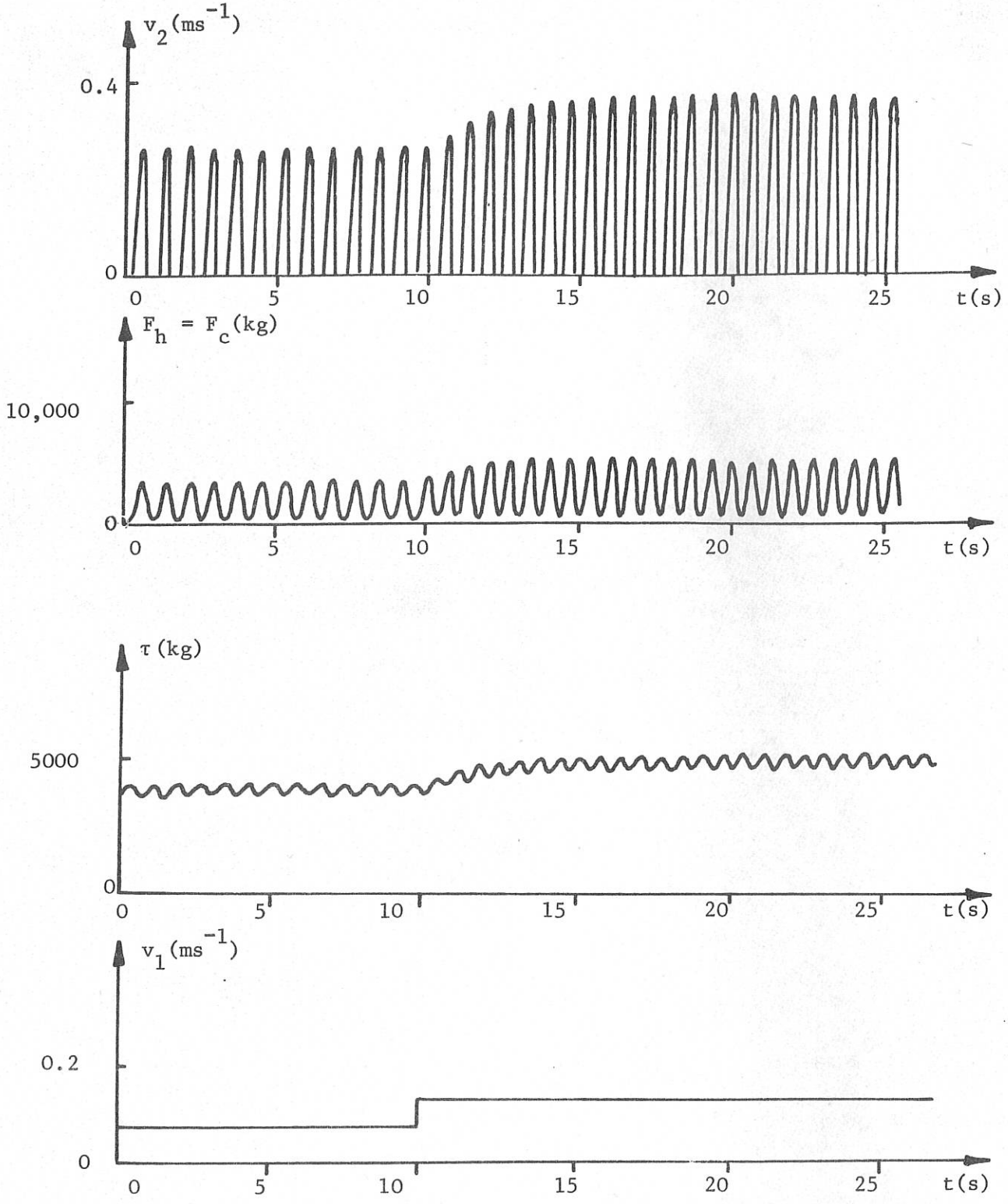

Fig. 13.6 Simulated performance of shearer machine (open-loop control)

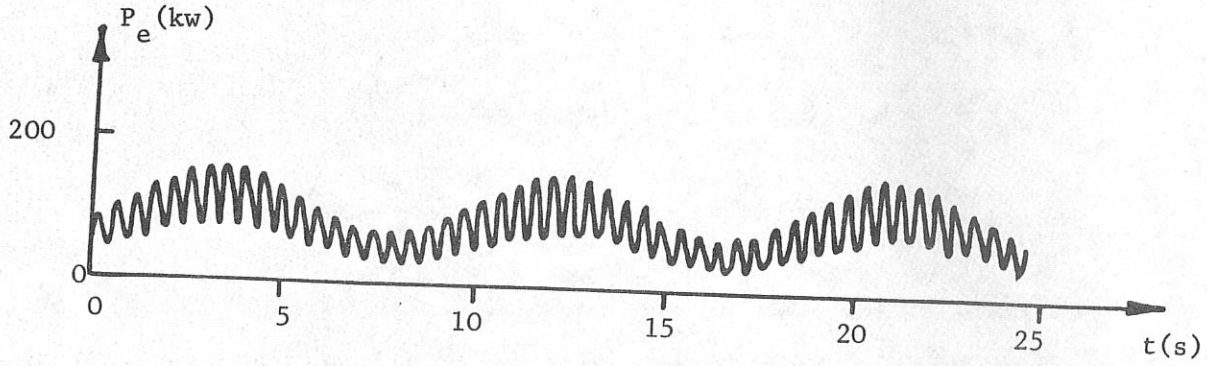

Fig. 13.7 Simulated power consumption of cutting drum drive (automatically cntrolled)

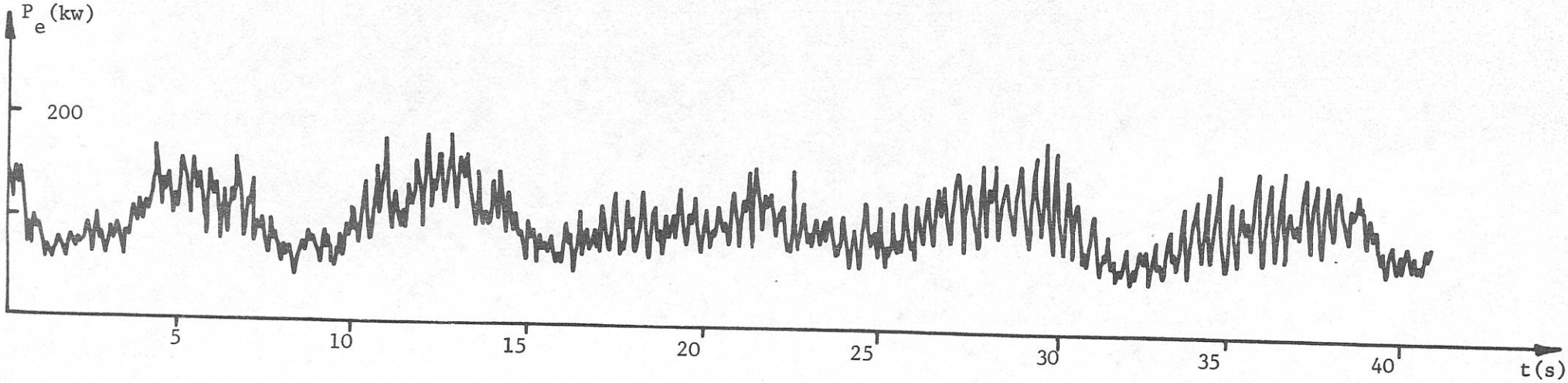

Fig. 13.8 Field recording of shearer drum drive power consumption (automatically controlled)

Fig. 13.9 Discontinuous oscillation

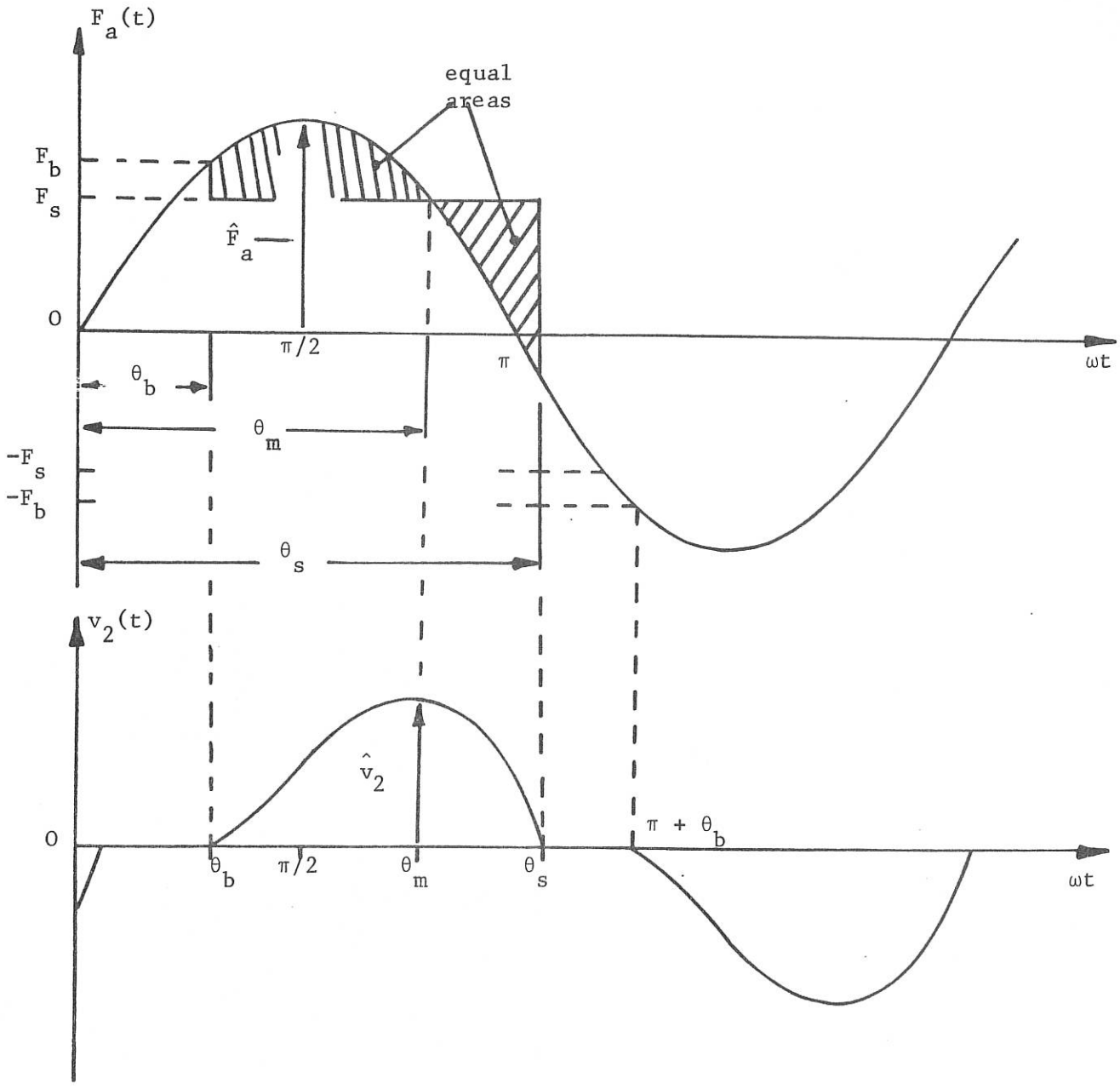

Fig. 13.10 Continuous Oscillation

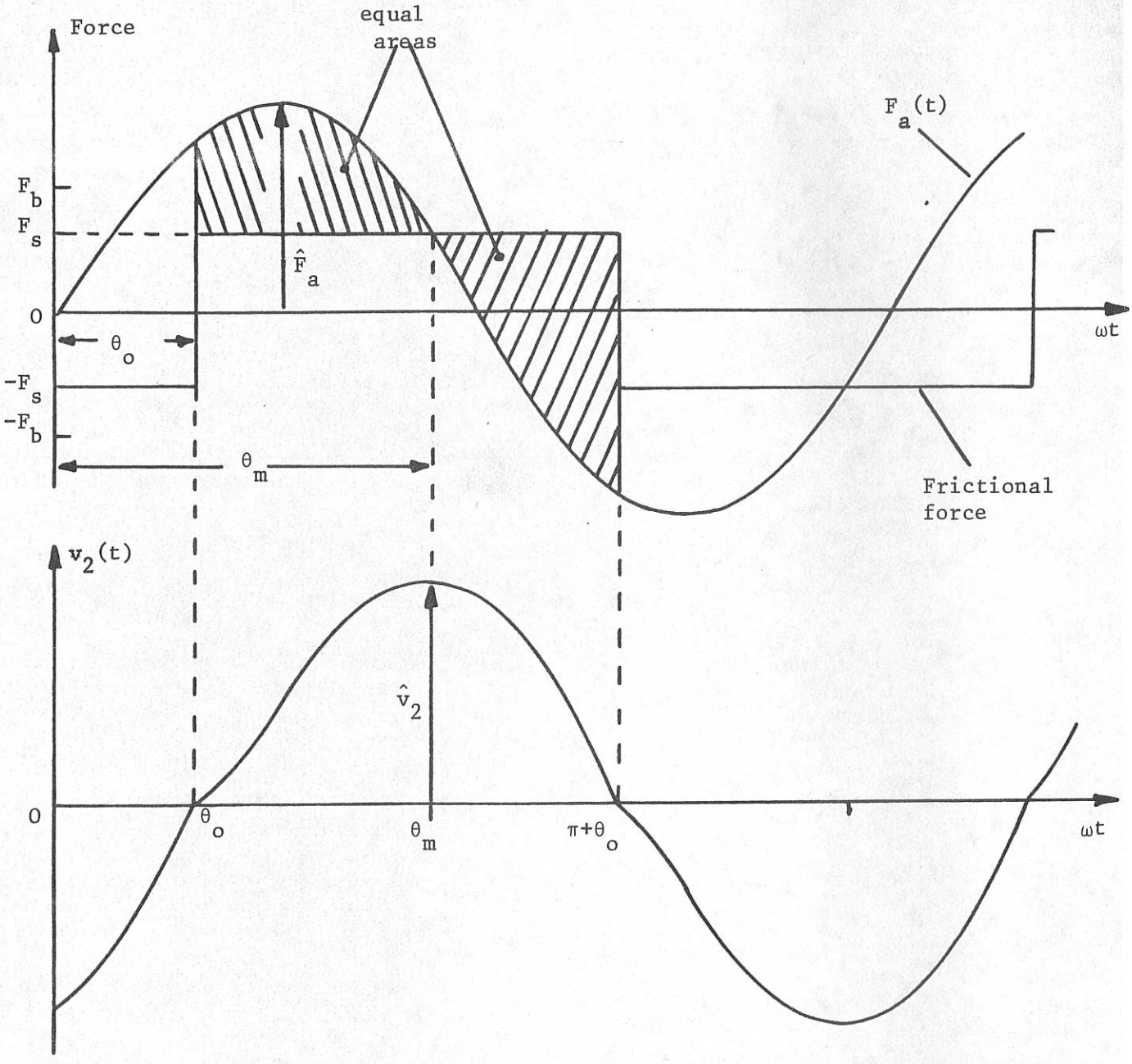

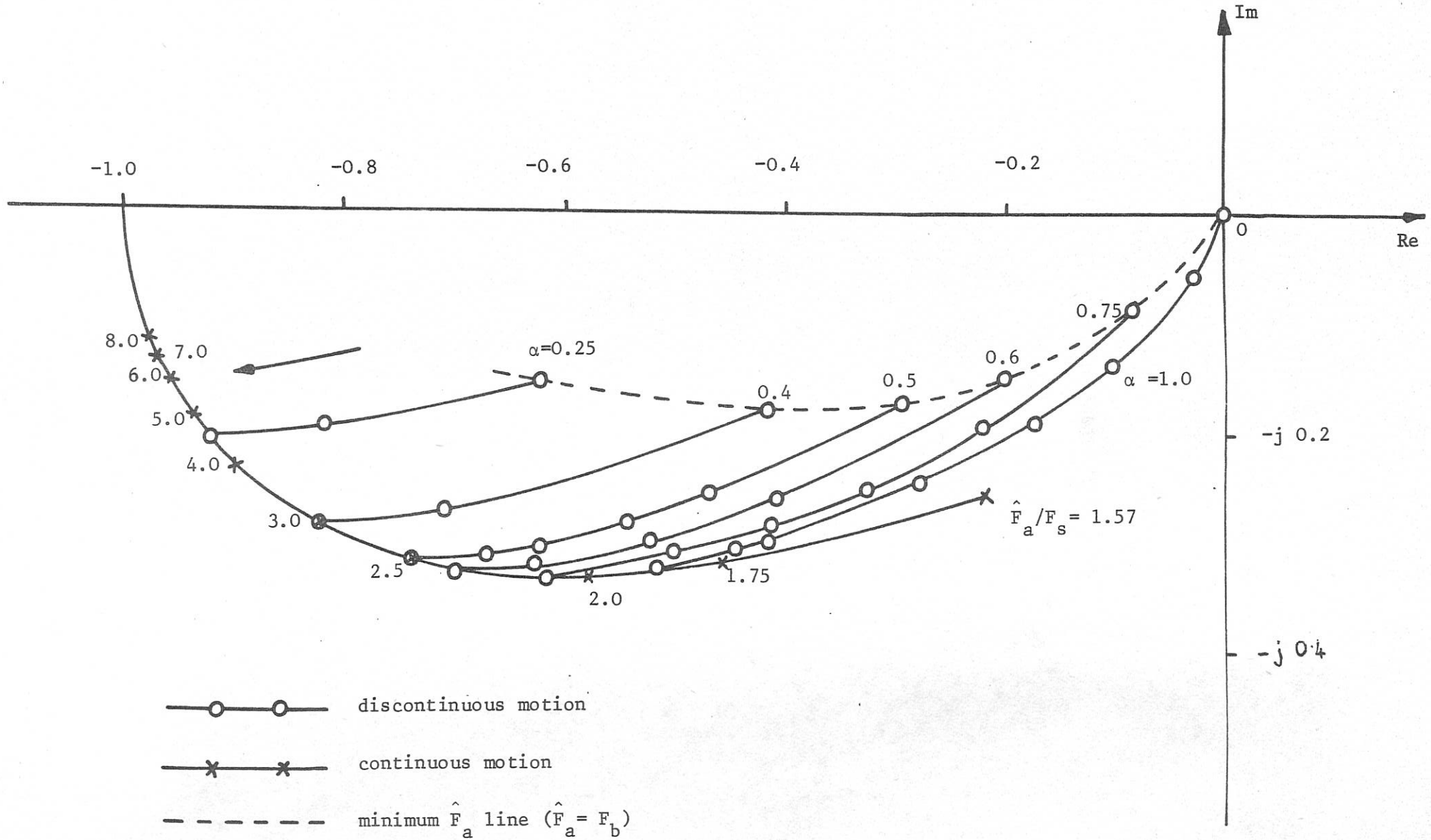

Fig. 13.11 Locus of $-G_F(\hat{F}_a, j\omega)$

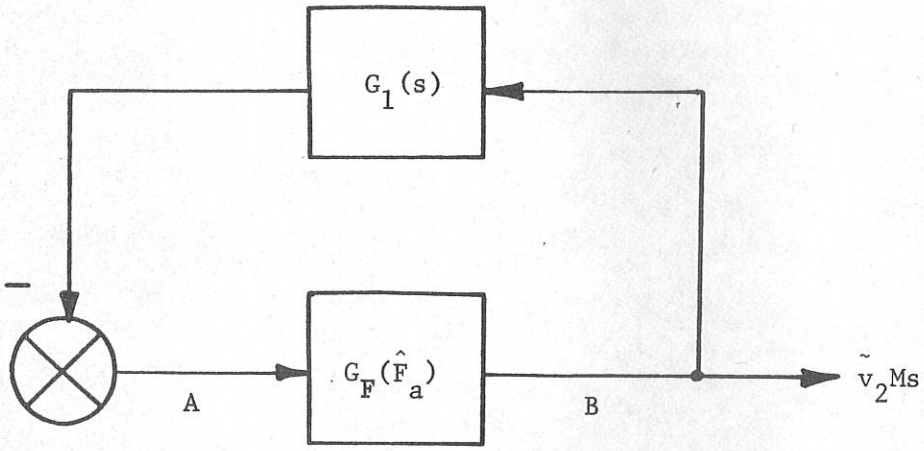

Fig. 13.12 Block-diagram reduced to a single loop

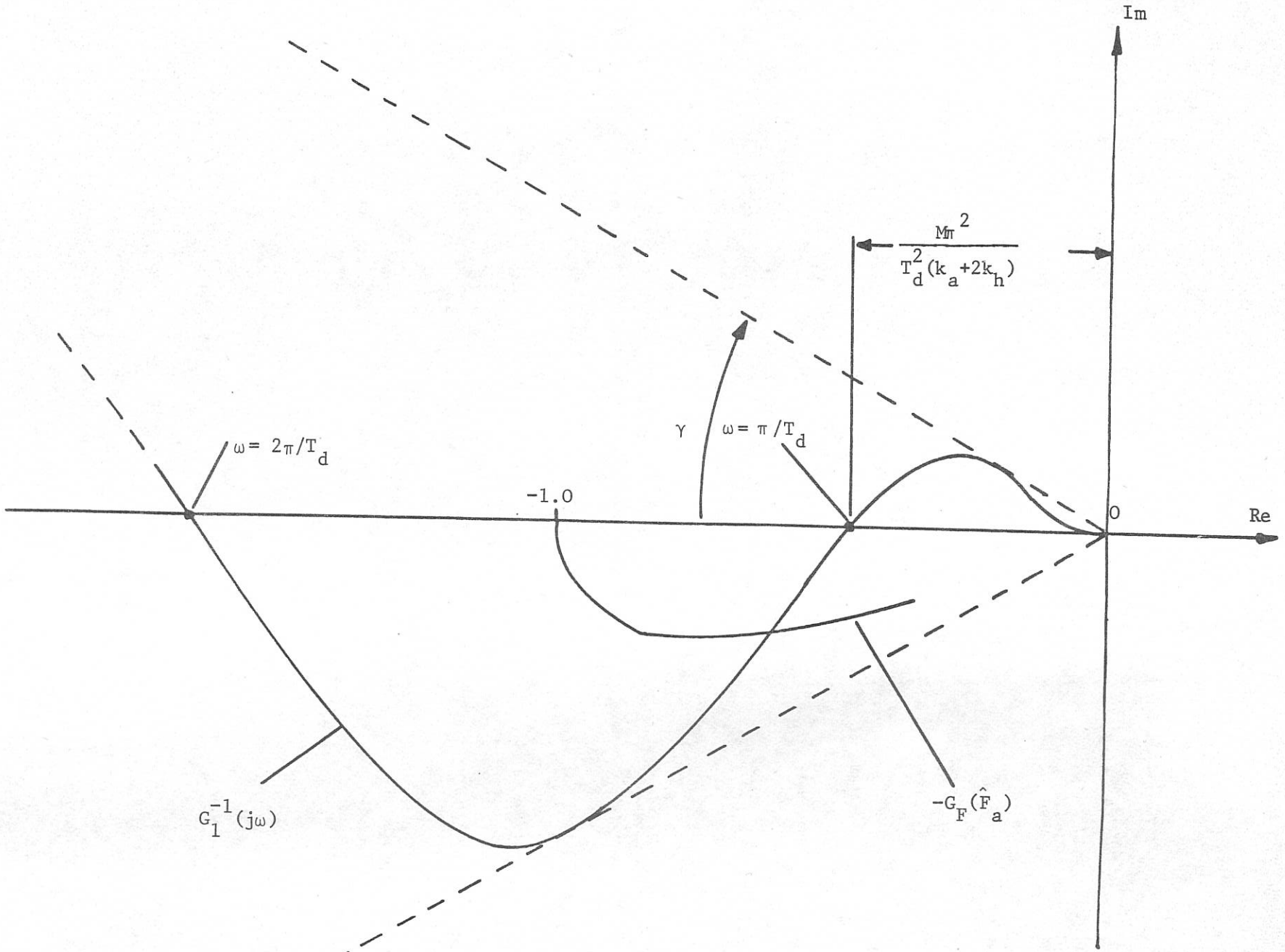

Fig. 13.13 General form of $G_1^{-1}(j\omega)$ locus

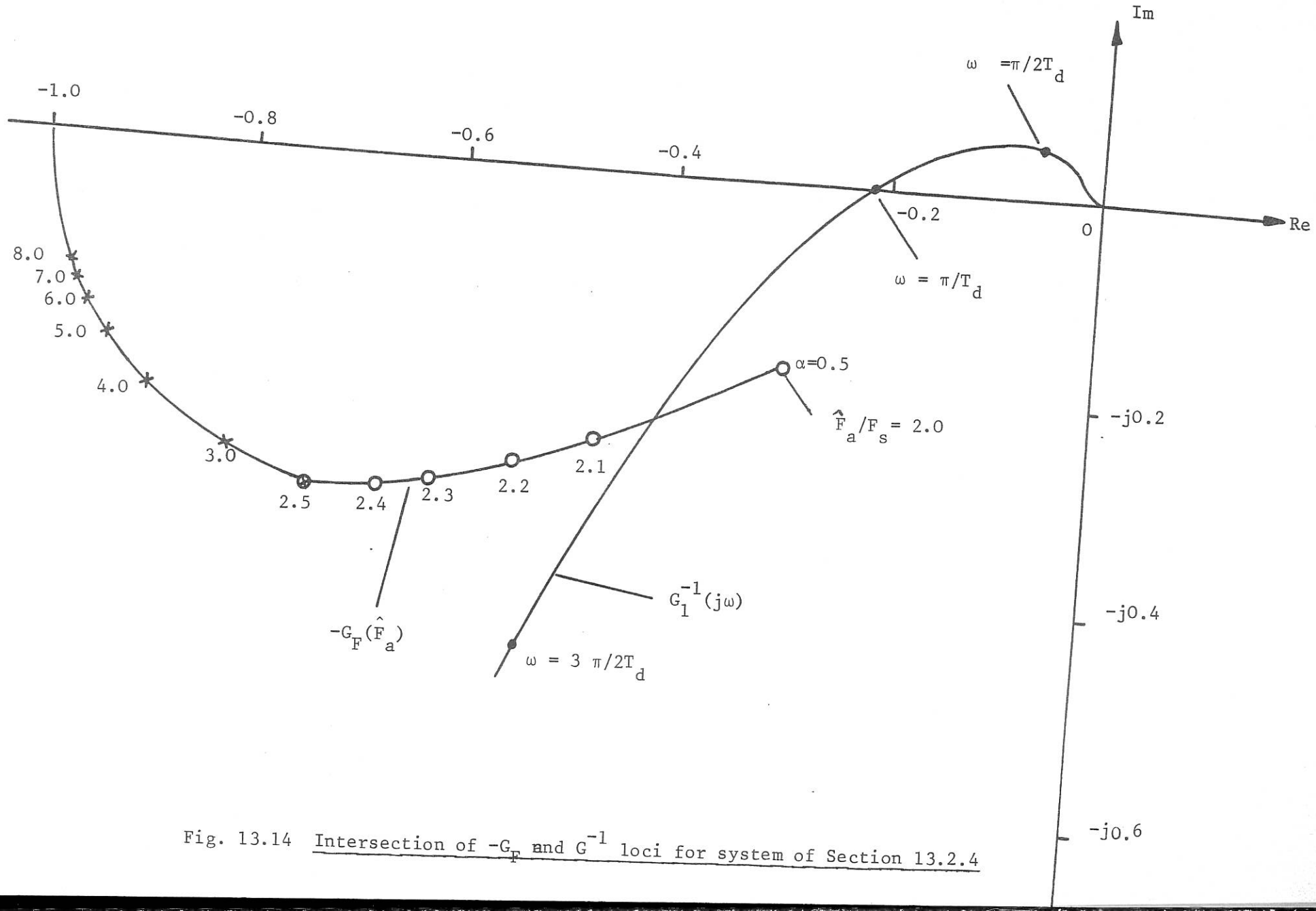

Fig. 13.14 Intersection of $-G_F$ and G^{-1} loci for system of Section 13.2.4

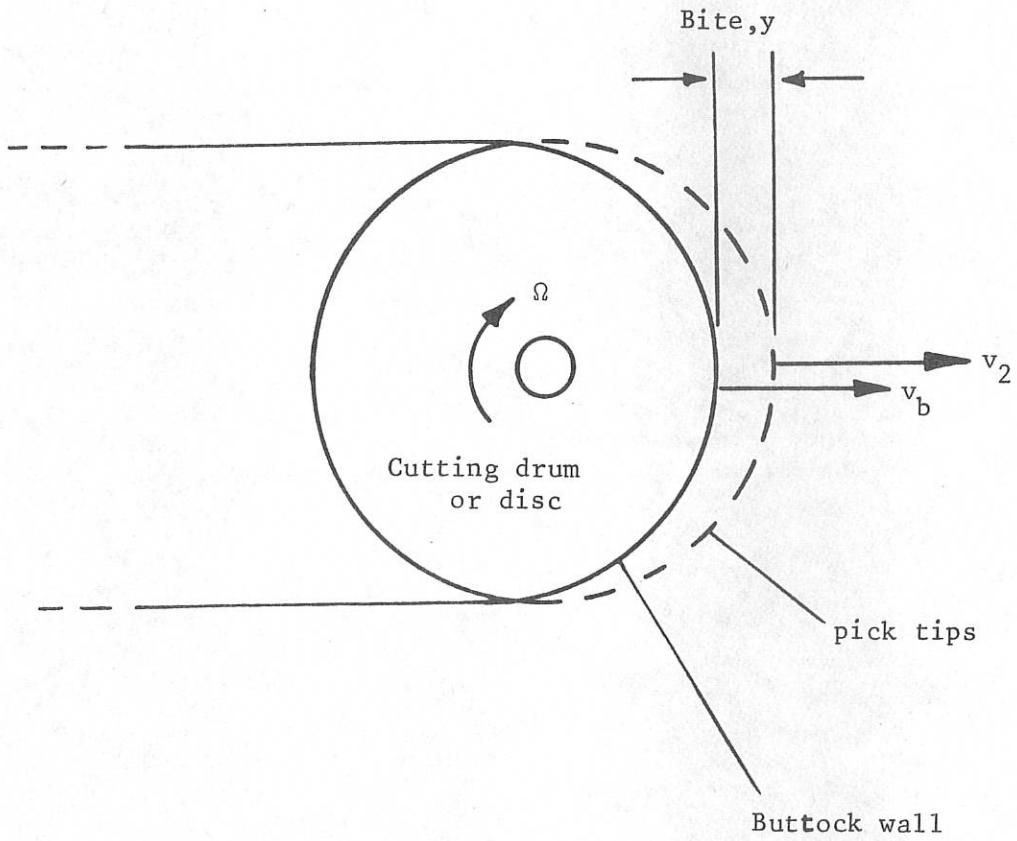

Fig. 13.15 Conceptual physical model for simplified treatment of cutting dynamics

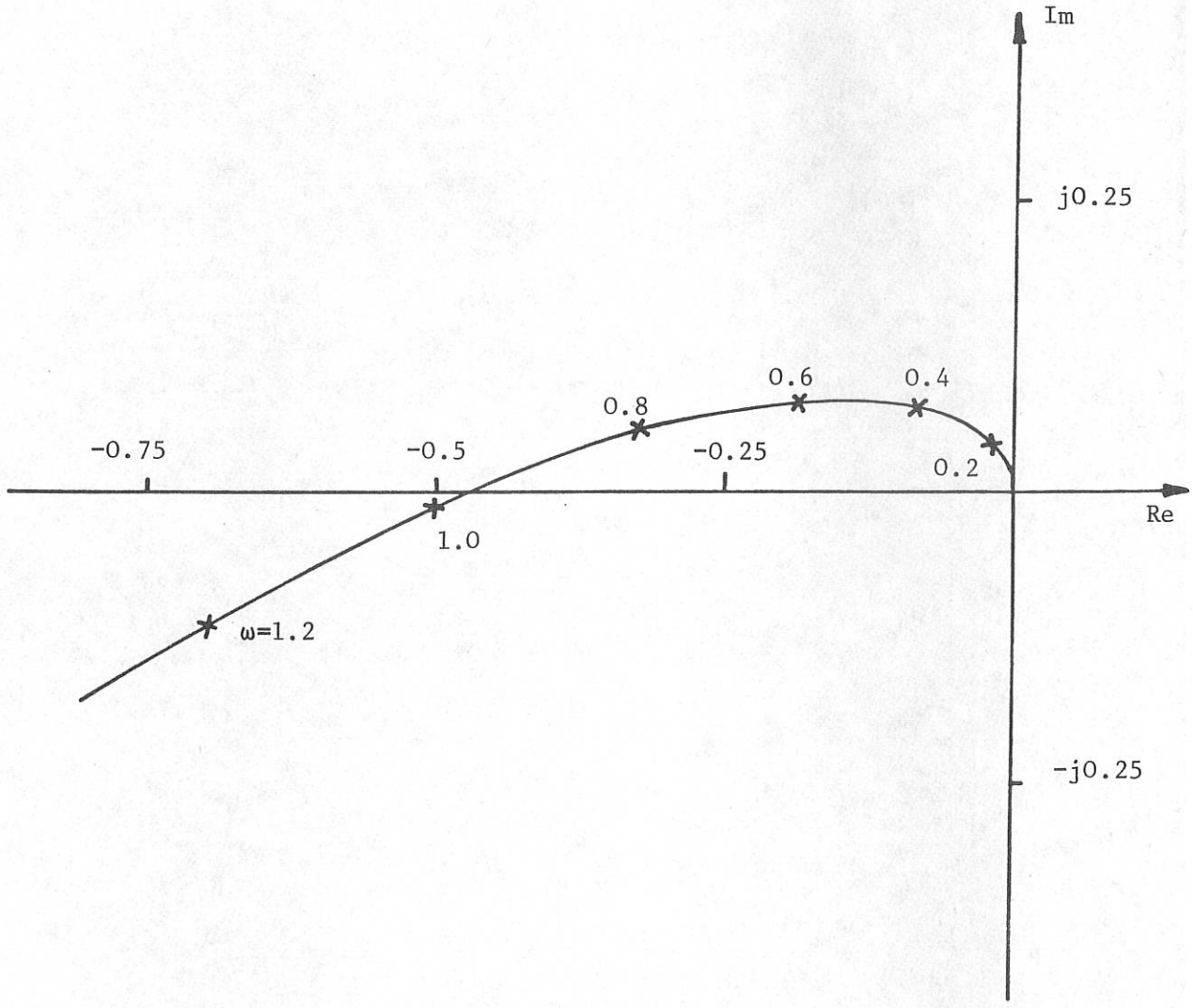

Fig. 13.16 Inverse Nyquist locus for low-frequency analysis

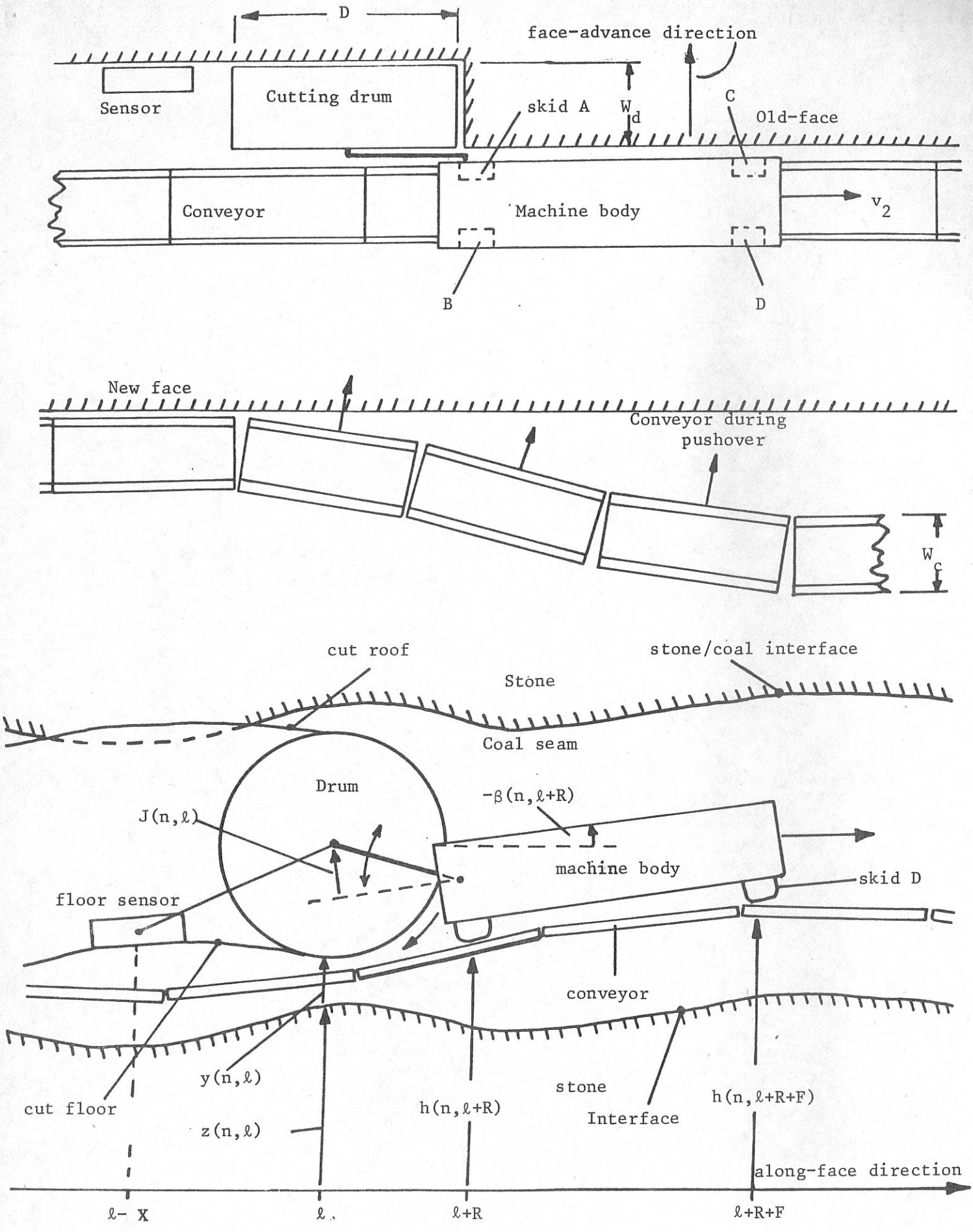

Fig. 13.17 Diagramatic plan and side-elevation of longwall shearer machine

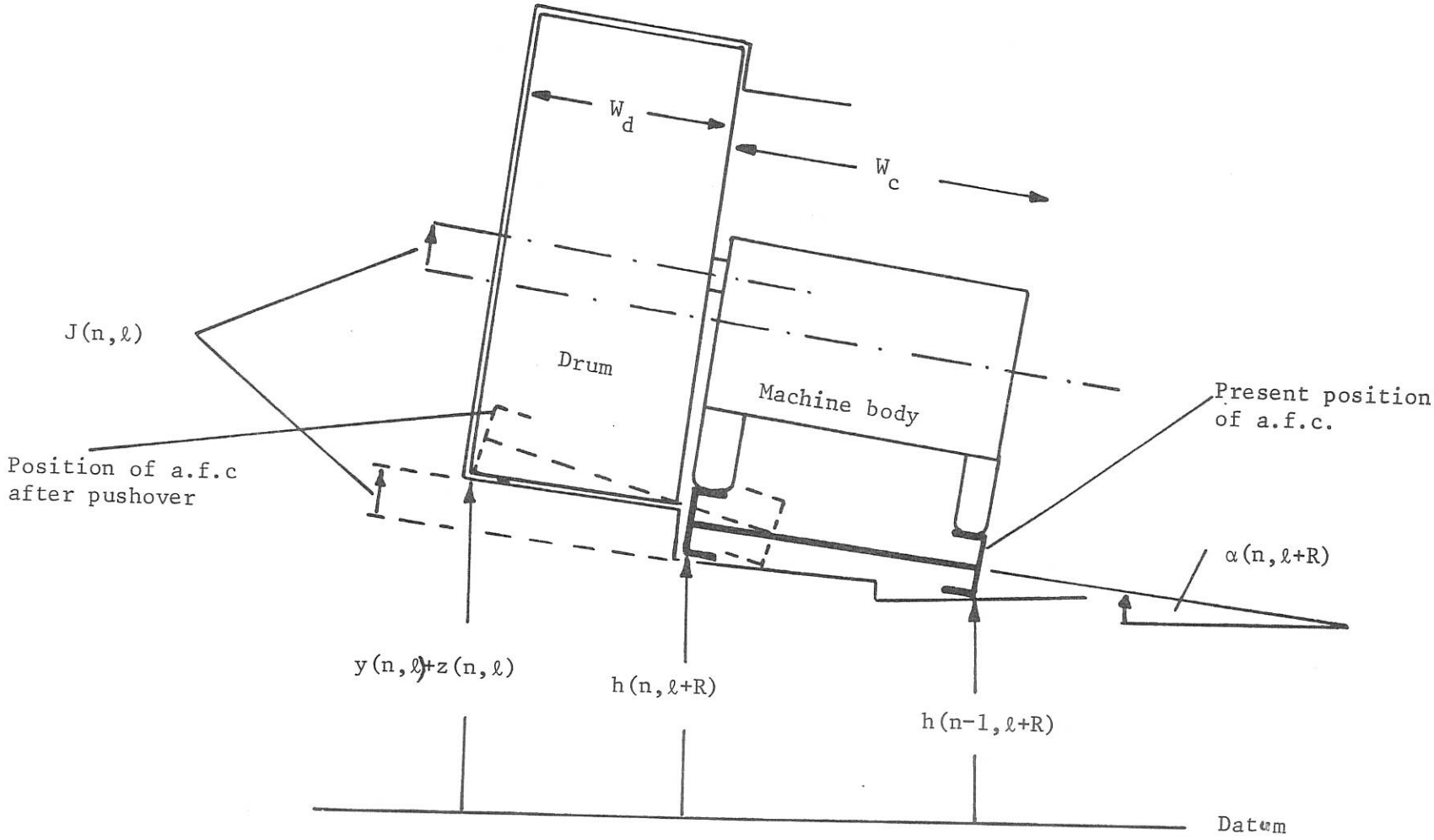

Fig. 13.18 Diagramatic end view of longwall shearer system.

Fig. 13.19 Simulated response of rubber-conveyor model to unit downward step in coal-seam

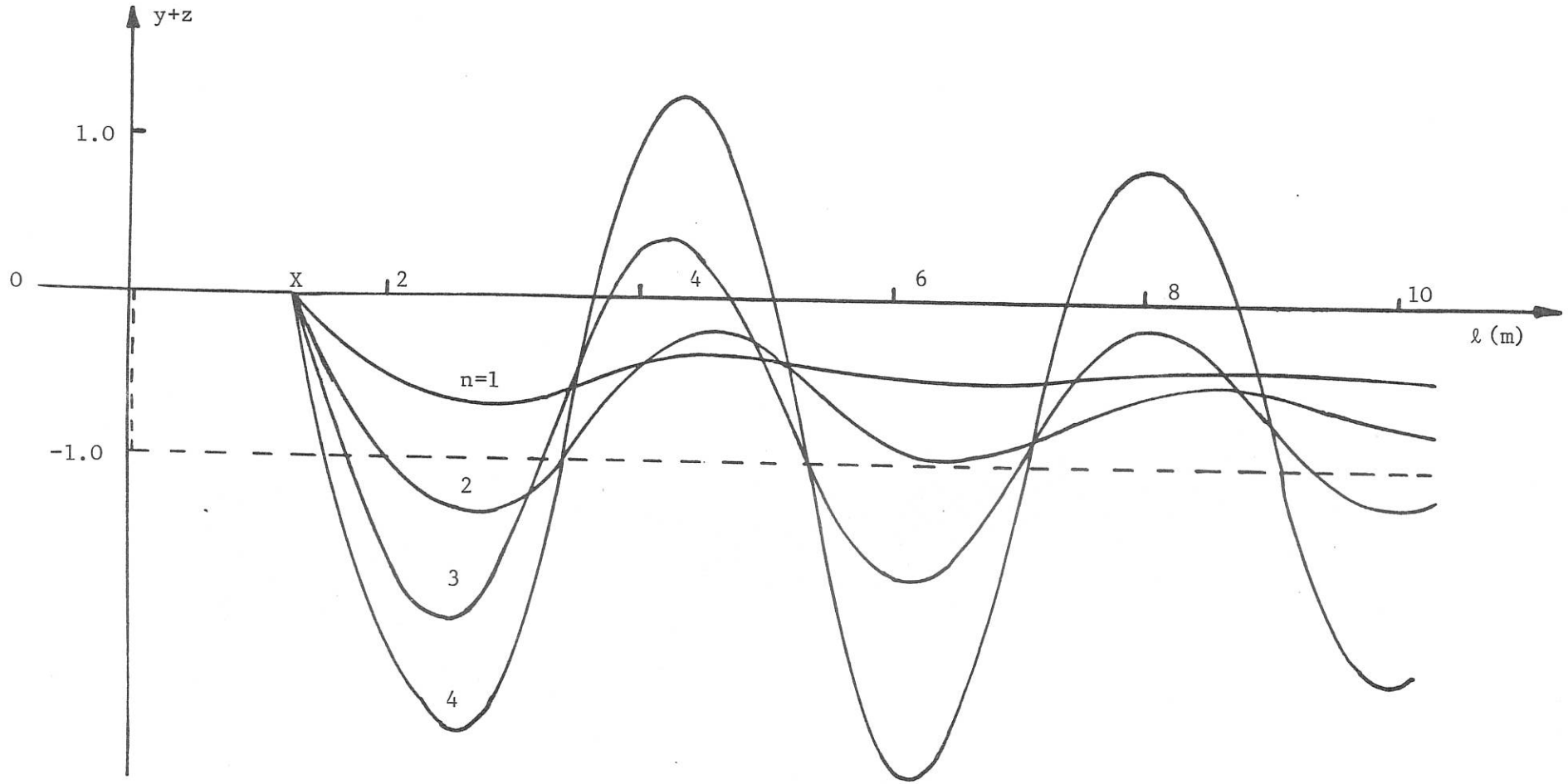

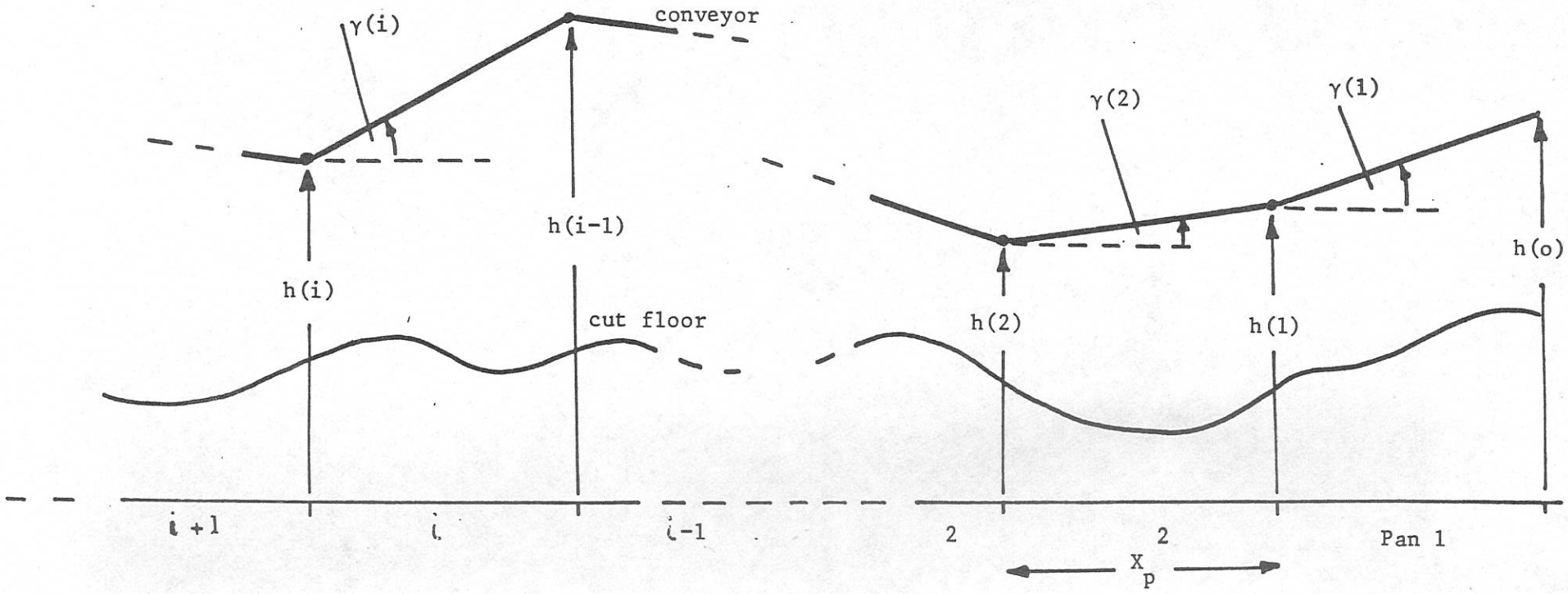

Fig. 13.20 Definition of variables for conveyor fitting problem.

Fig. 13.21 Flowchart for fitting i'th pan by dynamic programming

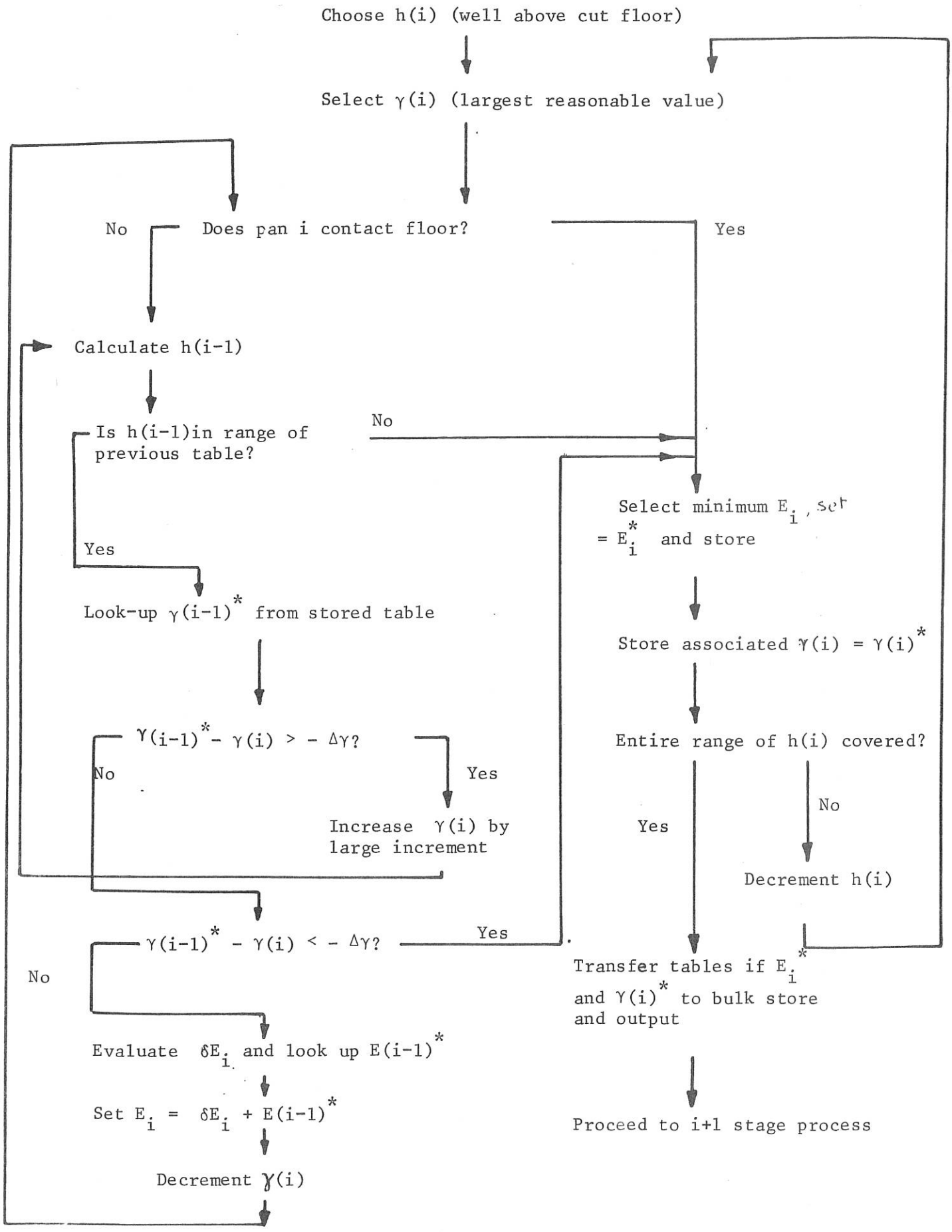

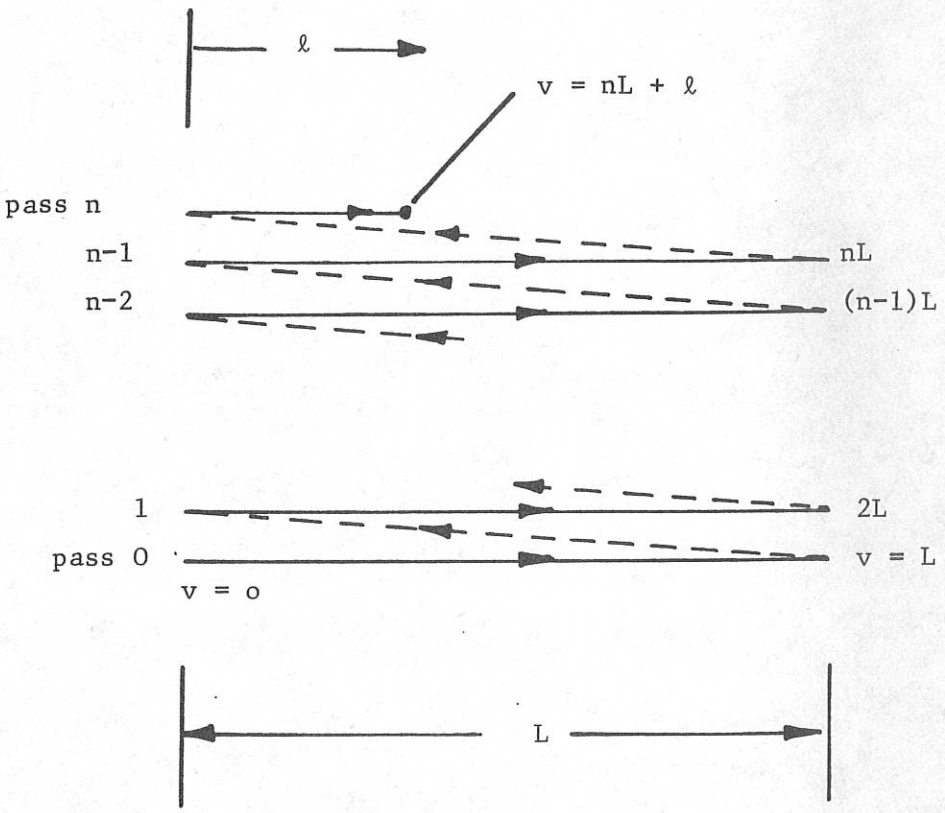

Fig. 13.22 Showing the accumulation of total distance passed, v, in a unidirectional multipass process

Process in operation

Process being 'reset'

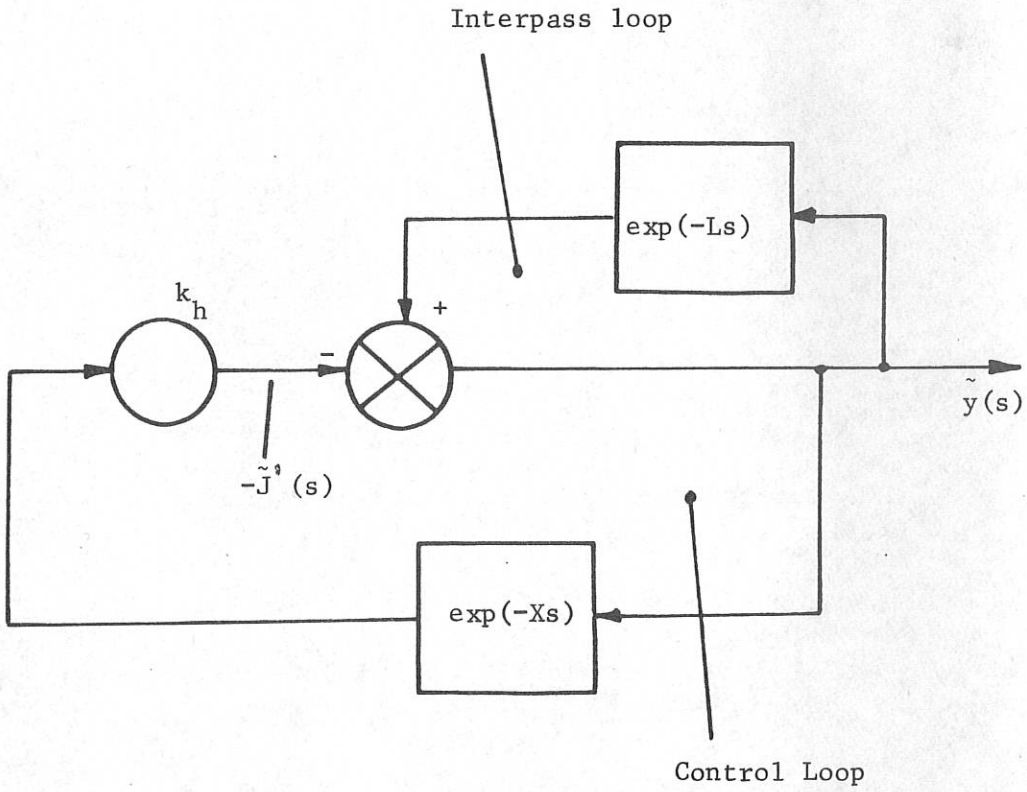

Fig. 13.23 Block diagram representation of simplified vertical steering system

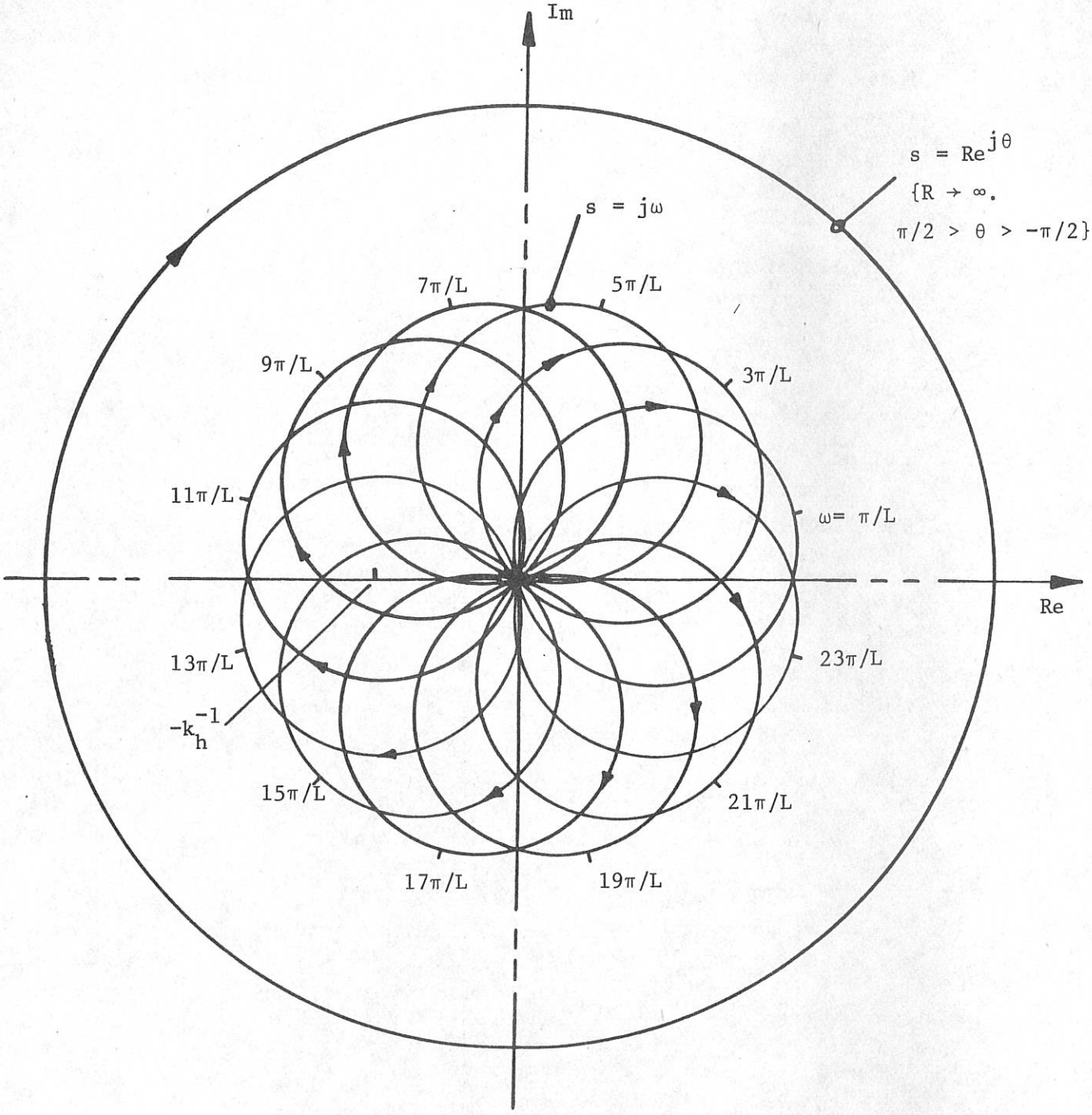

Fig. 13.24 Inverse Nyquist diagram for simplified vertical steering system

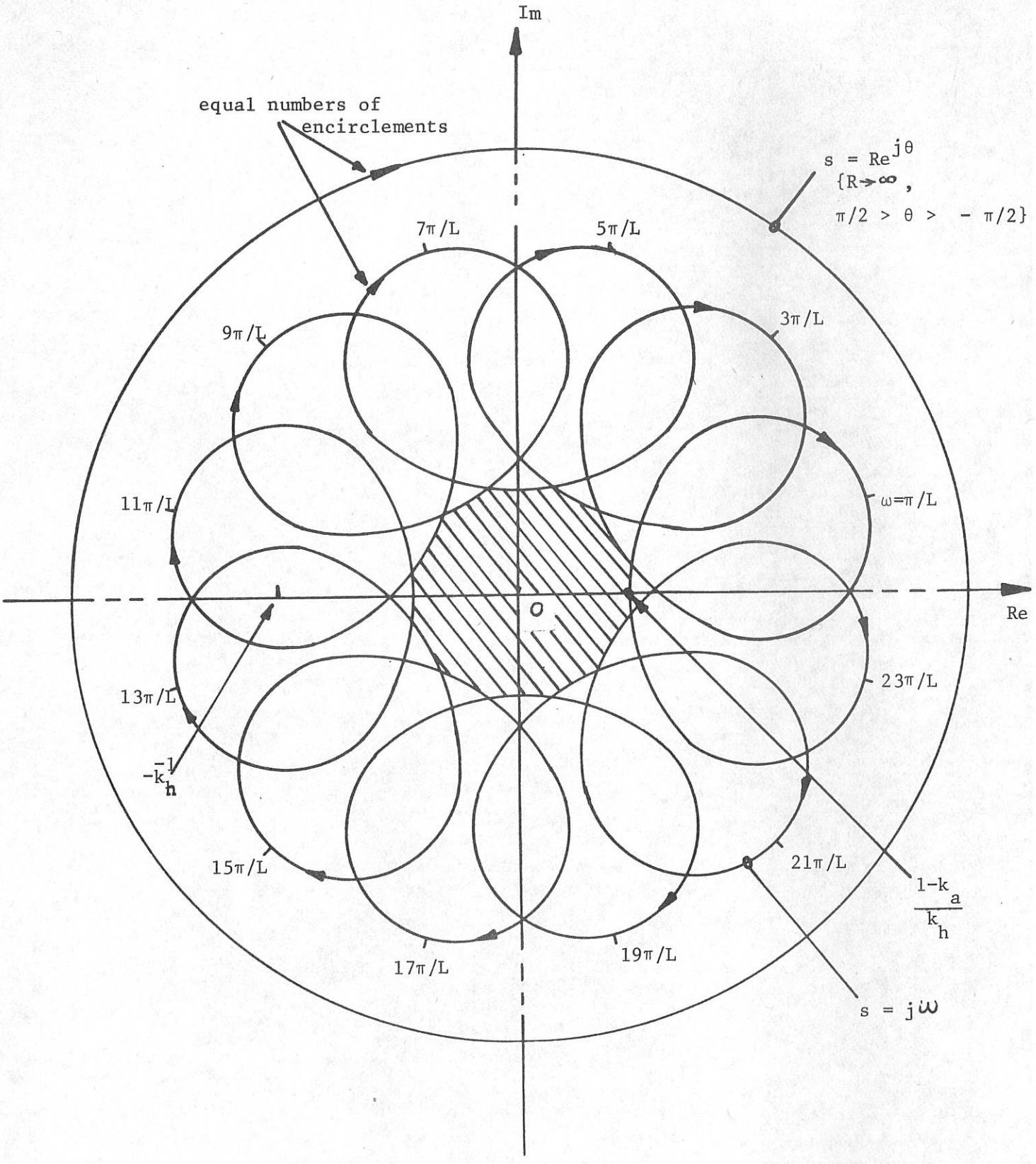

Fig. 13.25 Inverse Nyquist locus with constant interpass attenuation

Region of stability for siting -1.0 point

(a) Disturbance between pans

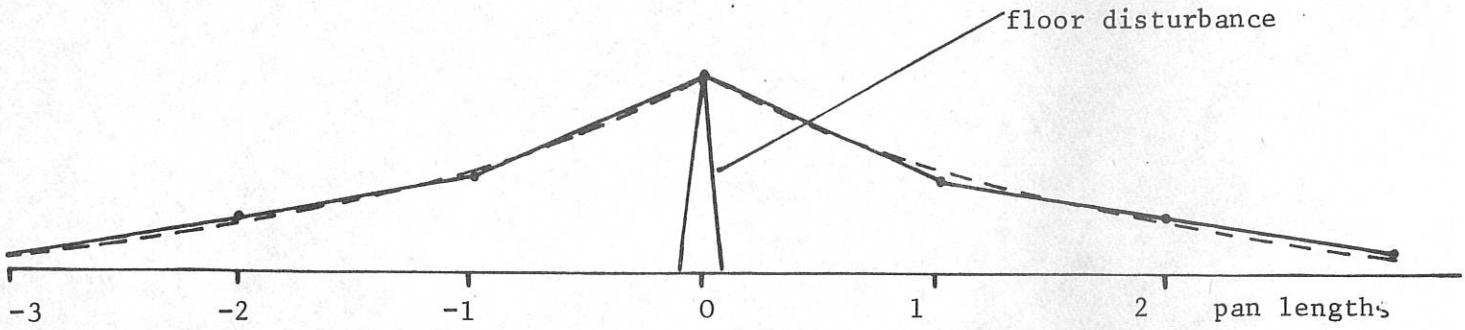

(b) Disturbance at pan-centre

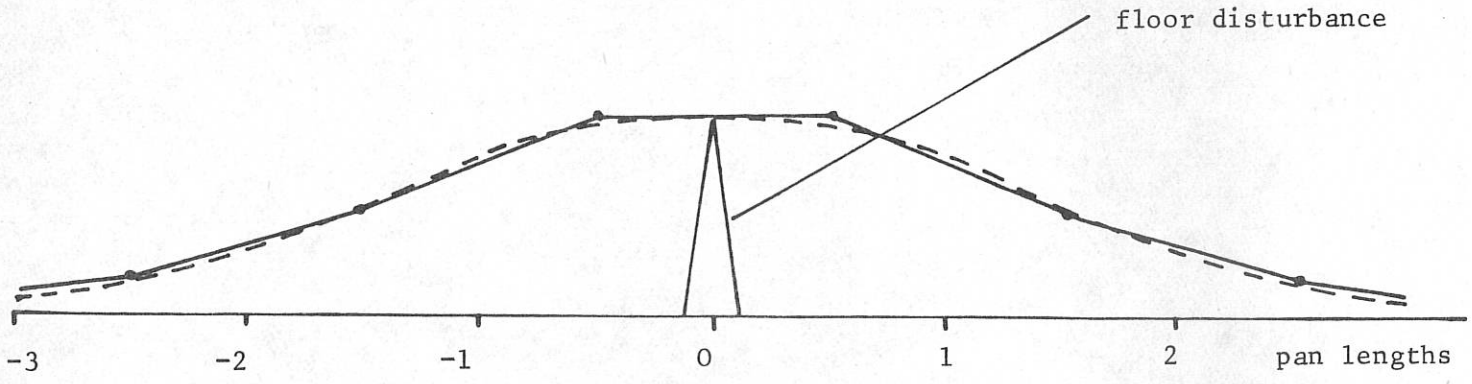

Fig. 13.26 Response of conveyor to a sharp disturbance in the cut floor

———— True conveyor shape

– – – – Continuous approximation

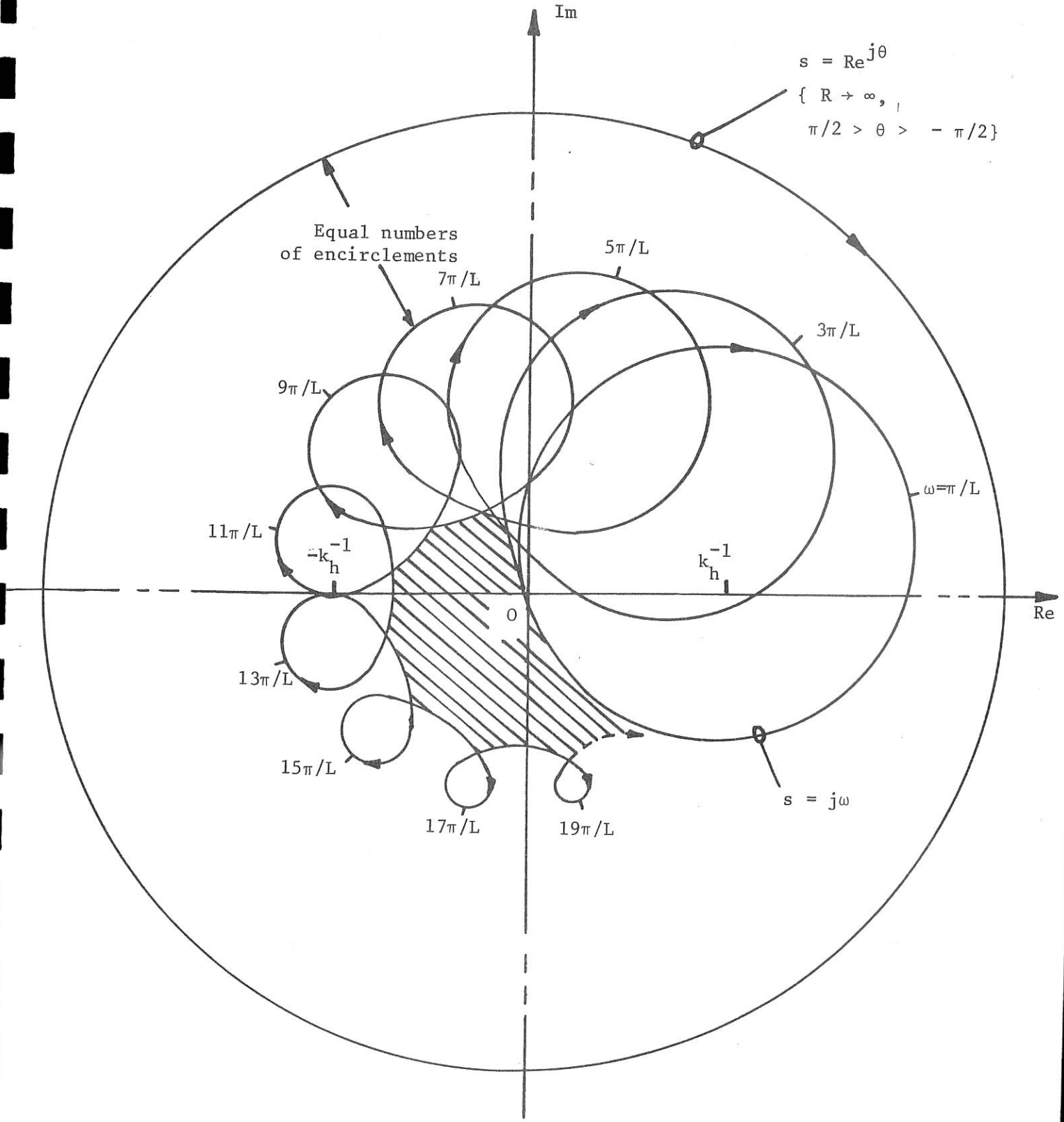

Fig. 13.27 Inverse Nyquist locus with first-order a.f.c model

Region of stability for siting -1.0 point

Fig. 13.28 Showing a simple clearance system

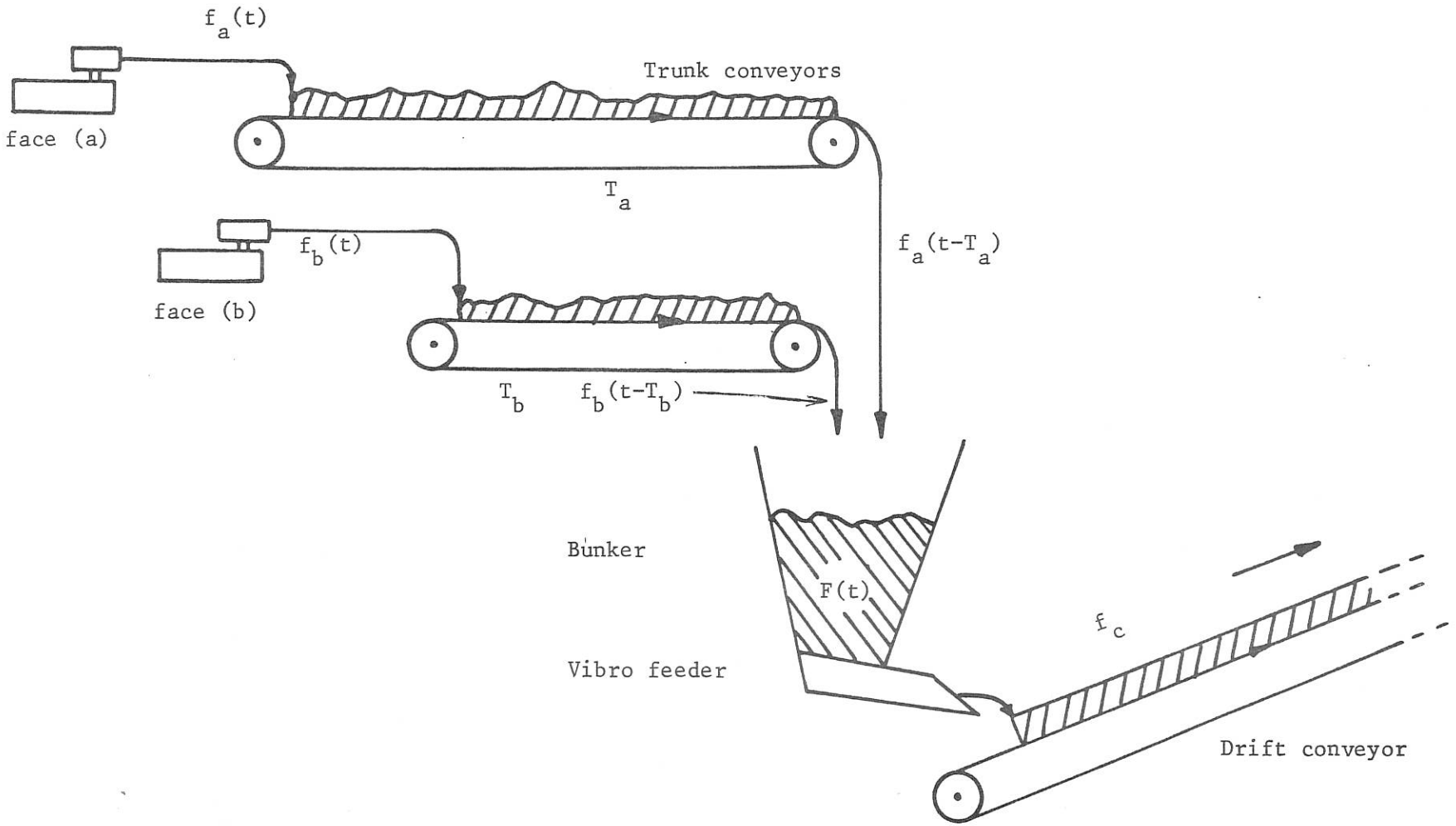

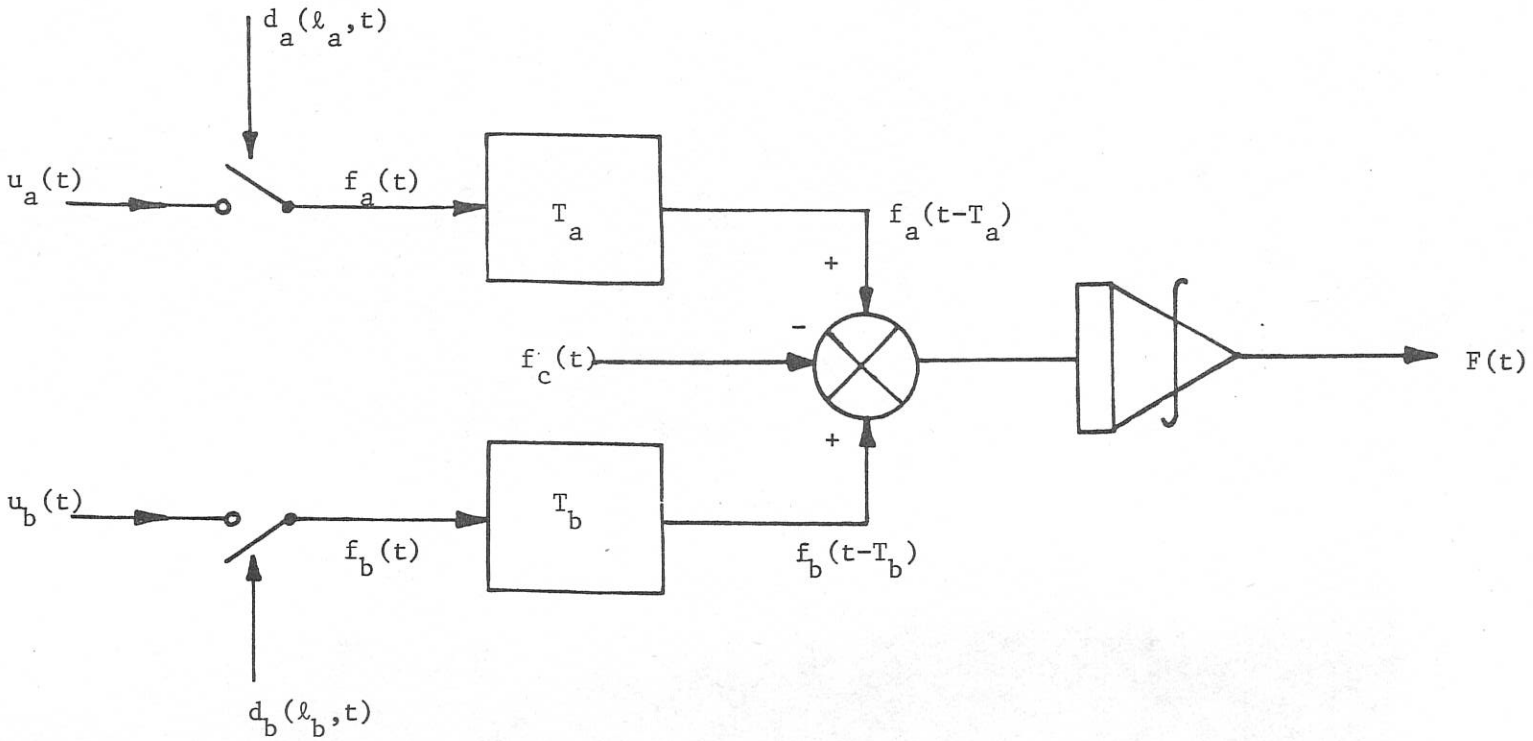

Fig. 13.29 Block diagram of clearance system of Fig. 13.30

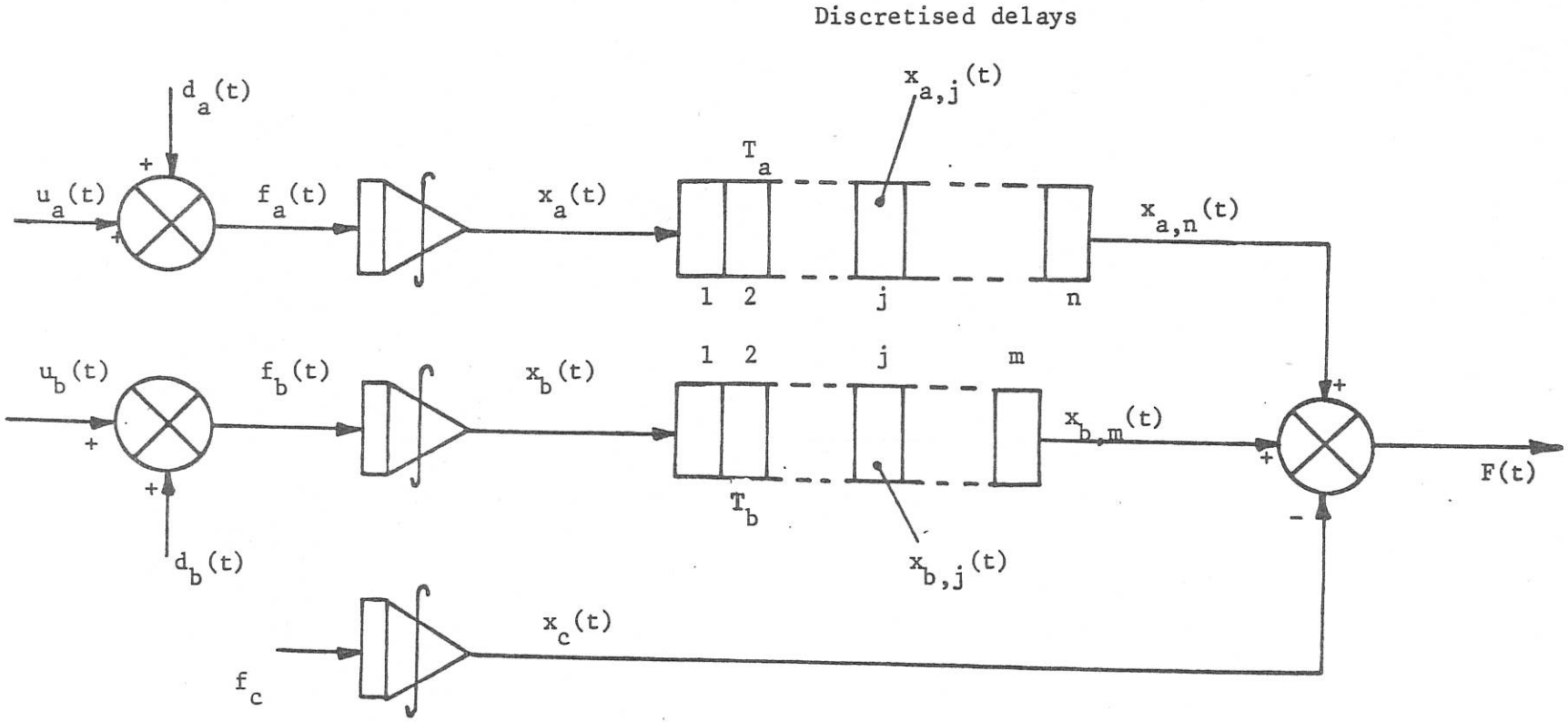

Fig. 13.30 Block diagram of clearance system modified for optimal control design

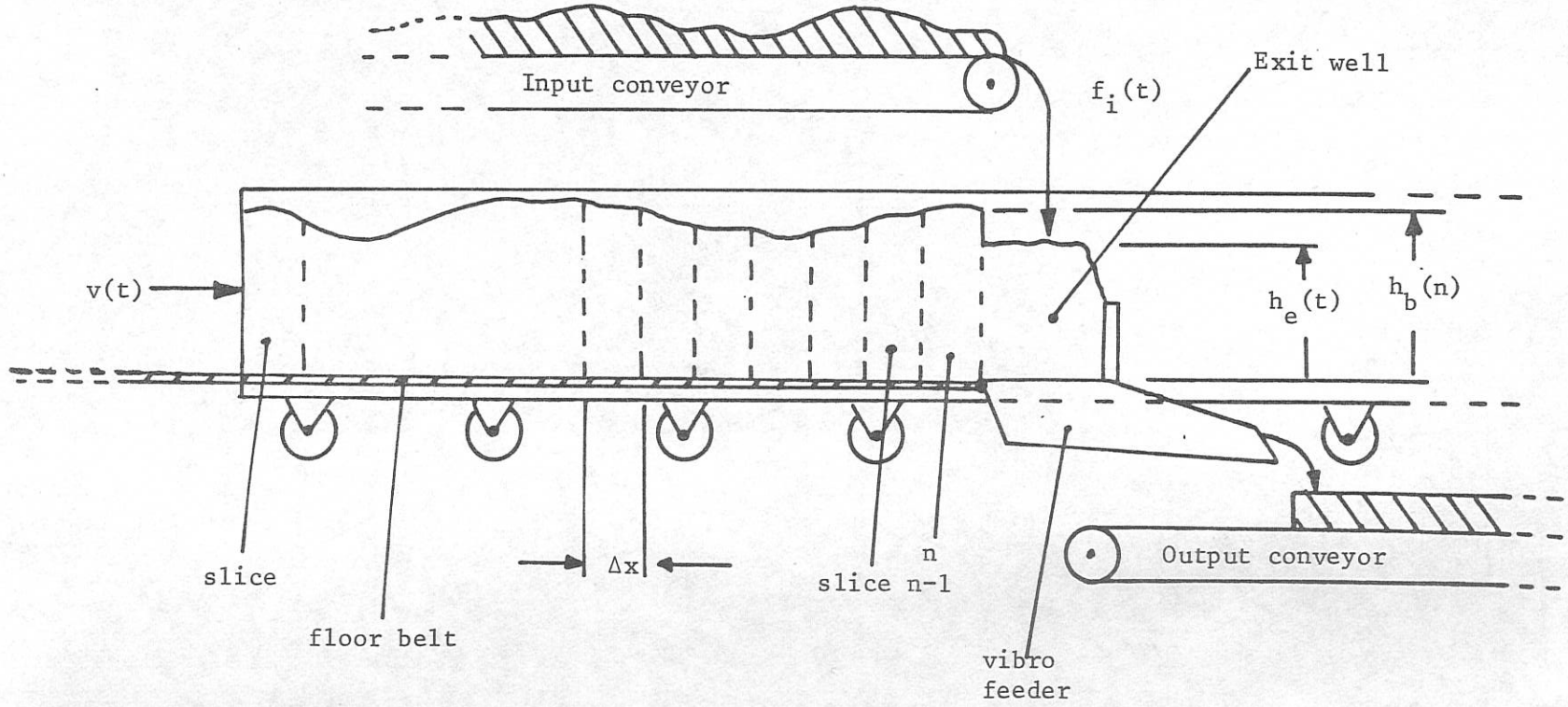

Fig. 13.31 Diagram of Bunker Conveyor

Fig. 13.32 Response of automatically controlled bunker to input flow changes